

GTA-HDR: A Large-Scale Synthetic Dataset for HDR Image Reconstruction

Hrishav Bakul Barua*, Kalin Stefanov, *Member, IEEE*, KokSheik Wong[†], *Senior Member, IEEE*, Abhinav Dhall, *Member, IEEE* and Ganesh Krishnasamy, *Member, IEEE*

Abstract—High Dynamic Range (HDR) content (*i.e.*, images and videos) has a broad range of applications. However, capturing HDR content from real-world scenes is expensive and time-consuming. Therefore, the challenging task of reconstructing visually accurate HDR images from their Low Dynamic Range (LDR) counterparts is gaining attention in the vision research community. A major challenge in this research problem is the lack of datasets, which capture diverse scene conditions (*e.g.*, lighting, shadows, weather, locations, landscapes, objects, humans, buildings) and various image features (*e.g.*, color, contrast, saturation, hue, luminance, brightness, radiance). To address this gap, in this paper, we introduce GTA-HDR, a large-scale synthetic dataset of photo-realistic HDR images sampled from the GTA-V video game. We perform thorough evaluation of the proposed dataset, which demonstrates significant qualitative and quantitative improvements of the state-of-the-art HDR image reconstruction methods. Furthermore, we demonstrate the effectiveness of the proposed dataset and its impact on additional computer vision tasks including 3D human pose estimation, human body part segmentation, and holistic scene segmentation. The dataset, data collection pipeline, and evaluation code are available at: <https://github.com/HrishavBakulBarua/GTA-HDR>.

Index Terms—High dynamic range imaging, tone mapping, inverse tone mapping, deep learning, machine learning

I. INTRODUCTION

HIGH Dynamic Range (HDR) [1] content (*i.e.*, images and videos) has been adopted widely in various domains including entertainment [2], gaming and augmented/virtual reality [3], medical imaging [4], computational photography [5], and robotics/robot vision [6]. However, capturing HDR content from real-world scenes is costly and time-consuming. Therefore, HDR image reconstruction from Low Dynamic Range (LDR) counterparts has been an active area of research in the last several years [7]–[12]. The literature proposes a multitude

of methods for HDR image reconstruction that are gradually shifting from traditional (non-learning) techniques [13]–[16] towards data-driven learning-based, such as Generative Adversarial Networks [17] and Diffusion Models [18].

Given that the performance of any data-driven learning-based method for HDR image reconstruction largely depends on the size and diversity of the datasets used for development, there is a significant gap in the publicly available datasets required to advance this research direction. Specifically, the existing datasets are either: 1) Not sufficiently large [19]–[25]; 2) Not having satisfactory resolution [26], [27]; 3) Having limited scene diversity [19], [24], [25]; 4) Having limited image variations [25], [28]–[30]; or 5) Absence of ground truth HDR images [31]–[33]. Furthermore, currently, there are no available datasets that adequately address the problem of no-reference HDR image quality assessment, which demands vast collections of ground truth HDR and distorted HDR pairs [34]–[36]. In summary, there is a substantial research gap pertaining to benchmark datasets needed to advance the research on HDR image reconstruction, hence motivating the creation of an appropriate large-scale dataset.

Video games have been used for creation and annotation of various large-scale datasets in diverse computer vision tasks [37] including 3D human pose and motion reconstruction [38], semantic segmentation [39], 3D scene layout and visual odometry [40], pedestrian detection and tracking [41], object detection and 3D mesh recovery [42], optical flow and depth estimation [43]. Drawing inspiration from the success of various data-driven learning-based methods developed with video game data, in this paper, we propose GTA-HDR, a large-scale synthetic dataset for HDR image reconstruction, sampled from the photo-realistic (*i.e.*, HDR-10¹ enabled) game Grand Theft Auto V² (GTA-V) by Rockstar Games³. Many game-inspired datasets for vision applications are constructed utilizing GTA-V. Previous work has also used other video games including Hitman [44], Witcher 3 [45], and Far Cry Primal [46] which contain highly realistic and detailed worlds with high fidelity. However, those games lack the diversity of scenes, which is the main trait of GTA-V.

We performed a thorough evaluation of the proposed dataset demonstrating important advantages it brings to the state-of-the-art in HDR image reconstruction including: 1) Using the GTA-HDR dataset in combination with other real and synthetic

H. B. Barua is with School of Information Technology, Monash University, and Robotics and Autonomous Systems Group, TCS Research, India (e-mail: hrishav.barua@monash.edu).

K. Stefanov is with Faculty of Information Technology, Monash University, Australia (e-mail: kalin.stefanov@monash.edu).

K. Wong is with School of Information Technology, Monash University, Malaysia (e-mail: wong.koksheik@monash.edu).

A. Dhall is with Flinders University, Adelaide, Australia, and Centre for Applied Research in Data Sciences, Indian Institute of Technology Ropar, India (e-mail: abhinav@iitrr.ac.in).

G. Krishnasamy is with School of Information Technology, Monash University, Malaysia (e-mail: ganesh.krishnasamy@monash.edu).

*This research is supported by the Global Excellence and Mobility Scholarship, Monash University.

[†]This research is supported, in part, by the E-Science fund under the project: *Innovative High Dynamic Range Imaging - From Information Hiding to Its Applications* (Grant No. 01-02-10-SF0327).

¹<https://en.wikipedia.org/wiki/HDR10>

²<https://www.rockstargames.com/gta-v>

³<https://www.rockstargames.com>

TABLE I: **Publicly available datasets for HDR image reconstruction.** See Section III-B for description of *In-the-wild*, *Scene diversity* and *Image diversity*; *GT*: Ground truth; *Dis*: Distorted; *: Minimum image resolution.

Dataset	Year	Type	#HDR _{GT}	Resolution	In-the-wild	HDR _{Dis}	Scene diversity	Image diversity
HDR-Eye [22]	2015	Synthetic	46	512 × 512	✗	✗	✗	✗
City Scene [26], [27]	2017	Mixed	41222	128 × 64	✗	✗	✓	✗
Kalantari <i>et al.</i> [19]	2017	Real	89	1500 × 1000	✗	✗	✗	✗
Endo <i>et al.</i> [20]	2017	Synthetic	1043	512 × 512	✗	✗	✗	✗
Eilertsen <i>et al.</i> [21]	2017	Synthetic	96	1024 × 768	✗	✗	✗	✗
Lee <i>et al.</i> [23]	2018	Synthetic	96	512 × 512	✗	✗	✗	✗
Cai <i>et al.</i> [29]	2018	Synthetic	4413	3072 × 1620*	✗	✗	✗	✗
Prabhakar <i>et al.</i> [24]	2019	Real	582	1200 × 900*	✗	✗	✗	✗
LDR-HDR Pair [25]	2020	Real	176	1024 × 1024	✗	✗	✗	✗
HDR-Synth & HDR-Real [28]	2020	Mixed	20537	512 × 512	✗	✗	✗	✓
SI-HDR [47], [48]	2022	Real	181	1920 × 1280	✗	✗	✓	✗
GTA-HDR (ours)	2024	Synthetic	40000	512 × 512 1024 × 1024	✓	✓	✓	✓

datasets enables significant improvements in the quality of the reconstructed HDR images; and 2) The GTA-HDR dataset fills a gap not covered by any of the publically available real and synthetic datasets and as such, contributes towards better generalization capabilities for HDR image reconstruction. The main contributions of this work can be summarized as follows:

- Proposing GTA-HDR, a novel large-scale synthetic dataset and data collection pipeline to complement existing real and synthetic datasets for HDR image reconstruction (see Section III).
- Performing thorough experimental validation using existing real and synthetic datasets and state-of-the-art methods to highlight the contribution of the proposed dataset to the quality of HDR image reconstruction and recovery of image details with high fidelity (see Section V).
- Demonstrating the contribution of the proposed dataset by illustrating its impact on the state-of-the-art in other computer vision tasks including 3D human pose estimation, human body part segmentation, and holistic scene segmentation (see Section V).

II. RELATED WORK

This section provides an overview of previous research on traditional (non-learning) techniques, data-driven learning-based methods, and datasets for HDR image reconstruction from single- and multi-exposed LDR images.

A. Inverse Tone Mapping

Tone mapping [49] is the process of mapping the colors of HDR images capturing real-world scenes with a wide range of illumination levels to LDR images appropriate for standard displays with limited dynamic range. Inverse tone mapping [7] is the reverse process accomplished with either traditional (non-learning) methods or data-driven learning-based approaches. Given the sensor irradiance E and the exposure time Δt , the function $f_{crf}(E\Delta t)$ represents the tone mapping process, which outputs I_{LDR} images given I_{HDR} images captured by the camera sensor. The main goal of any HDR image reconstruction technique is to reverse the tone mapping process using another function $f_{crf}^{-1}(I_{LDR})/\Delta t$, which outputs reconstructed \hat{I}_{HDR} images given I_{LDR} im-

ages. The main challenge is that the steps in $f_{crf}(E\Delta t)$ are generally not reversible [50]. We can, however, approximate the reverse process with a data-driven learning-based model $f_{DL}(I_{LDR}, \Theta)$, which reconstructs \hat{I}_{HDR} images given I_{LDR} images, where Θ denotes the model parameters. An illustration of the tone mapping pipeline and the process of inverse tone mapping is provided in the Supplementary Material.

1) Non-Learning Methods

Luzardo *et al.* [13] described an inverse tone mapping operator that allows higher peak brightness (*i.e.*, over 1000 nits) while converting LDR images to HDR counterparts. The process helps preserve the artistic intent of the reconstructed HDR images. Kovaleski and Oliveira [14] focused on enhancing the over- and under-exposed regions of images using cross-bilateral filtering. Huo *et al.* [15] presented an inverse tone mapping technique based on the human visual system. The approach uses human retina response to model the inverse local retina response using local luminance adaptation in the image. Masia *et al.* [16] tried to address the ill-exposed areas of input LDR images, which are more prone to generate artifacts. This method uses an automatic global reverse tone mapping operator based on gamma expansion along with automatic parameter calculation based on image statistics. Bist *et al.* [51] proposed a gamma correction-based approach that adapts to the target lighting styles of the images. This work also added a color correction-based operator that reconstructs the intended colors in the HDR image.

2) Learning-Based Methods

Khan *et al.* [52] proposed a feedback mechanism based on a Convolutional Neural Network to generate HDR images from single-exposed LDR inputs. Barua *et al.* [53] utilized multi-exposed features and perceptual losses along with low- and mid-level feature guidance in generating visually accurate HDR images. Le *et al.* [50] leveraged a Neural Network-based camera response inversion architecture to generate pixel radiance and hallucination details for various exposures. Liu *et al.* [28] proposed an architecture consisting of three Convolutional Neural Networks that approximates the three sub-tasks in the tone mapping process but in the reverse order. Li

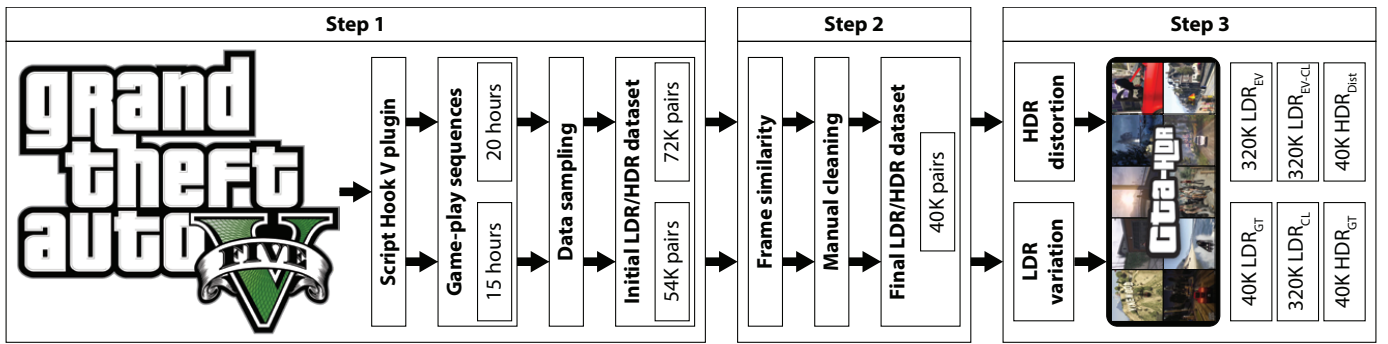


Fig. 1: **GTA-HDR dataset collection pipeline.** See Section III-A for detailed description of the three steps; *GT*: Ground truth; *Dis*: Distorted; *EV*: Exposure value; *CL*: Contrast level. *Note*: The GTA-V logo is retrieved from Google Images.

and Fang *et al.* [54] presented a combination of an attention mechanism and a Convolutional Neural Network that can recover over- and under-exposed regions of LDR images. Santos *et al.* [55] leveraged a feature masking mechanism that helps in reconstructing saturated pixels of LDR images resulting in better visual and perceptual quality of the reconstructed HDR images. Eilertsen *et al.* [21] proposed a Convolutional Neural Network for accurate prediction of HDR pixels from the complex under- and over-exposed counterparts in input LDR images. Luzardo *et al.* [56] tried to overcome the low peak brightness issues in the reconstructed HDR images to enhance the artistic intent. Cao *et al.* [57] proposed a method that combines the outputs of preliminary HDR results from a channel-decoupled kernel and pixel-wise output from another architecture resulting in high-quality HDR images. Jang *et al.* [25] explored the concept of the histogram and color differences between HDR and LDR pairs of multiple exposures to reconstruct HDR images.

Recently Neural Radiance Fields [58] were used to learn implicit color and radiance fields and perform photo-realistic HDR view synthesis [4]. The literature also provides examples of proposed video-based approaches [59] using various learning-based methods including Generative Adversarial Networks and Convolutional Neural Networks. Finally, some methods primarily deal with dynamic scenes [19], while others address multiple tasks, *e.g.*, denoising, deblurring, super-resolution, and demosaicing [60], and fuse them into an HDR image reconstruction pipeline.

B. Datasets

In the last several years there has been a shift in the research on HDR image reconstruction from traditional (non-learning) methods to data-driven learning-based approaches based on Generative Adversarial Networks [61], Convolutional Neural Networks [62], Diffusion Models [18], and Neural Radiance Fields [4]. These data-driven techniques require a significant amount of training data drawing attention to the limitations of the current publicly available datasets. Table I summarizes existing public datasets.

1) Real Datasets

Real datasets [19], [24], [25], [31]–[33], [47], [48] include images with sufficient resolution, however, their main limita-

tion is their size (*i.e.*, low number of images). It is difficult, time-consuming, and costly to collect real-world data using an HDR camera that covers a variety of scenes (*e.g.*, indoor, outdoor, in-the-wild), lightning conditions, and image characteristics (*e.g.*, different levels of contrast, radiance, saturation). The RAISE dataset [33] consists of real images and is of moderate size but it lacks ground truth HDR images and therefore is applicable for evaluation purposes only.

2) Synthetic Datasets

Synthetic datasets [20]–[23], [29], on the other hand, provide ground truth HDR images, however, only a few consist of large amounts of images. In addition, these datasets generally lack images with appropriate resolution and diversity. Although the synthetic video dataset proposed in [30] is originally designed for the development of super-resolution video generation methods, it can potentially support the development of data-driven learning-based HDR image reconstruction methods after appropriate data pre-processing.

3) Mixed Datasets

Several datasets [26]–[28] include images from both real and synthetic scenes. These datasets provide a sufficient amount of ground truth HDR images, however, they lack appropriate image resolution and diversity.

4) Proposed Dataset

The proposed GTA-HDR dataset addresses the identified gaps in the current publicly available datasets for HDR image reconstruction. Specifically: 1) GTA-HDR is a large-scale (*i.e.*, 40K ground truth HDR images) synthetic dataset sampled from the GTA-V video game data which utilizes ray tracing [63] technology to simulate the physics behind light and shadows; 2) GTA-HDR includes HDR images with sufficient resolution (*i.e.*, 512×512 and 1024×1024), and; 3) GTA-HDR includes HDR images capturing a diverse set of scenes including different locations (*e.g.*, indoor, urban, rural, in-the-wild), different lighting conditions (*e.g.*, morning, midday, evening, night), and different weather and season conditions (*e.g.*, summer, winter, snowy, rainy, sunny, cloudy).

C. No-Reference Quality Assessment

Due to the lack of ground truth HDR images and high costs of resource-demanding full-reference quality metrics [64] such

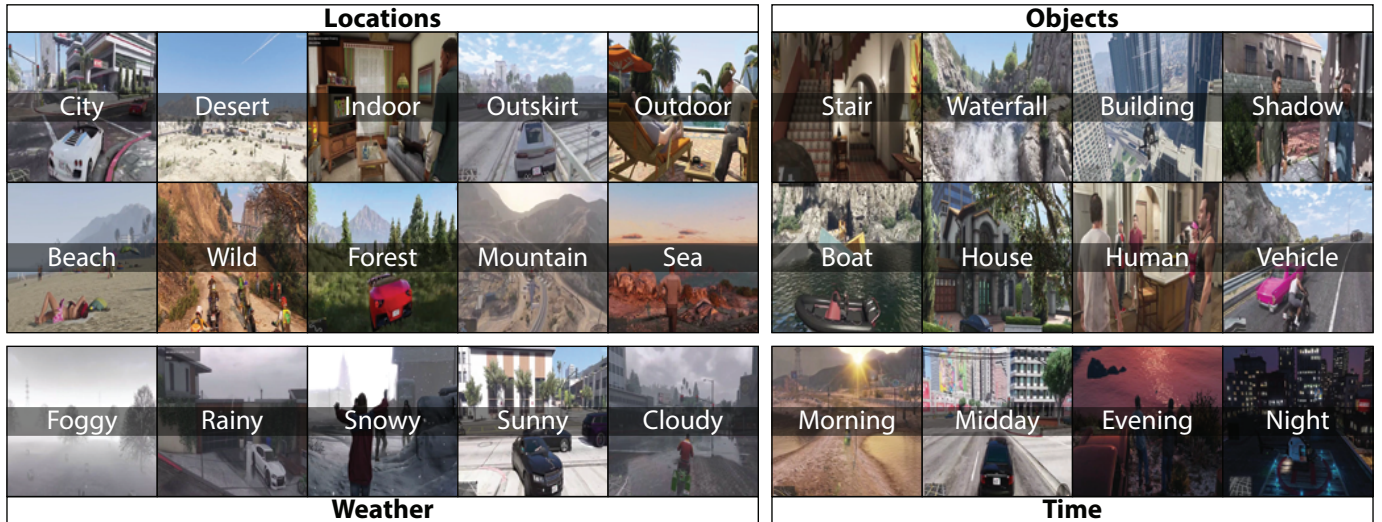


Fig. 2: **GTA-HDR dataset scene diversity.** Samples from the GTA-HDR dataset with multiple variations in location, weather, objects and time. The scene diversity ensures a thorough coverage of pixel colors, brightness, and luminance.

as High Dynamic Range Visual Differences Predictor [65], research has also accelerated in the field of no-reference HDR image quality assessment [35], [66]. Several approaches have tried to approximate the High Dynamic Range Visual Differences Predictor score for perceptual quality assessment of reconstructed HDR images using data-driven learning-based methods, such as Convolutional Neural Networks [34]–[36]. Other approaches have tried to approximate general quality score metrics of images (HDR or LDR), such as Peak Signal-to-Noise Ratio and Structural Similarity Index Measure, using Convolutional Neural Networks and distortion maps [67].

The GTA-HDR dataset also contributes a set of distorted HDR images along with the ground truth HDR and LDR images, which addresses the limitations of current datasets concerning no-reference image quality assessment for both HDR and tone-mapped HDR and LDR images.

III. GTA-HDR DATASET

The GTA-HDR dataset addresses some of the limitations of the existing datasets for HDR image reconstruction. The main characteristics of GTA-HDR are the diversity of scenes and variety of images included in the dataset (*e.g.*, forests, mountains, coasts, cities). GTA-HDR includes scenes from different times (*e.g.*, morning, evening, day-time, night) and different weather conditions (*e.g.*, rainy, snowy, sunny, misty). This variety of scenes is an expensive and effort-demanding task to collect in a real-world context. To our knowledge, this work is the first to use video game data to collect and curate synthetic {LDR/HDR} image pairs to support the development of inverse tone mapping data-driven methods.

A. Dataset Collection

We performed a thorough data collection and curation, adopting a similar approach as described in [37]. We used 2 full game-play sequences (*i.e.*, playing the story from the beginning until the end) from the GTA-V game to extract {LDR/HDR} image pairs at multiple resolutions (*i.e.*, $512 \times$

512 and 1024×1024). GTA-V has built-in HDR-10 support for displaying video sequences on HDR displays. Fig. 1 depicts the entire data collection pipeline for GTA-HDR.

In line with [37], we used Script Hook V⁴ plugin to capture HDR frames from the GTA-V game-play sequences. Other available tools for GTA-V game data extraction include RenderDoc Debugger⁵ and customized RenderDoc for the Game Data platform⁶. The normal duration of a GTA-V game-play is approximately 31.5 hours (*i.e.*, going through all basic aspects of the story), and it can extend up to about 82 hours (*i.e.*, visit all aspects of the story thoroughly). We collected data from 2 game-play sequences, one of around 15 hours and another of approximately 20 hours. During game data extraction, we sampled 1 frame per second. This results in approximately 54K and 72K {LDR/HDR} image pairs, respectively.

The steps followed in the data collection process are as follows (see Fig. 1): 1) We used Script Hook V to extract {LDR/HDR} image pairs with 1Hz frequency, which yielded 54K and 72K pairs; 2) We removed frames that are similar to the previous or next frames in the sequence to avoid unnecessary increase in dataset size and redundant information. The similarity between two consecutive frames in the sequence is based on [68]; we discarded frames that have a similarity score higher than 0.8. We also did a manual cleaning of the collected data to remove unwanted scenes (*e.g.*, images containing violence and other objectionable actions or items). Finally, we ensured that the collected data has an even distribution of scenes from indoor, outdoor, and in-the-wild environments, resulting in a total of 40K {LDR/HDR} pairs; and 3) We performed transformations on the original LDR images to generate multiple exposure LDR images (*i.e.*, exposure values EV 0, ± 1 , ± 2 , ± 3 , and ± 4) [50] and different contrast levels [29]. This step results in $40K \times 25 = 1M$ LDR images. Apart from the 40K original HDR images, we

⁴<http://www.dev-c.com/gtav/scripthookv/>

⁵<https://github.com/baldurk/renderdoc>

⁶https://github.com/xiaofeng94/renderdoc_for_game_data

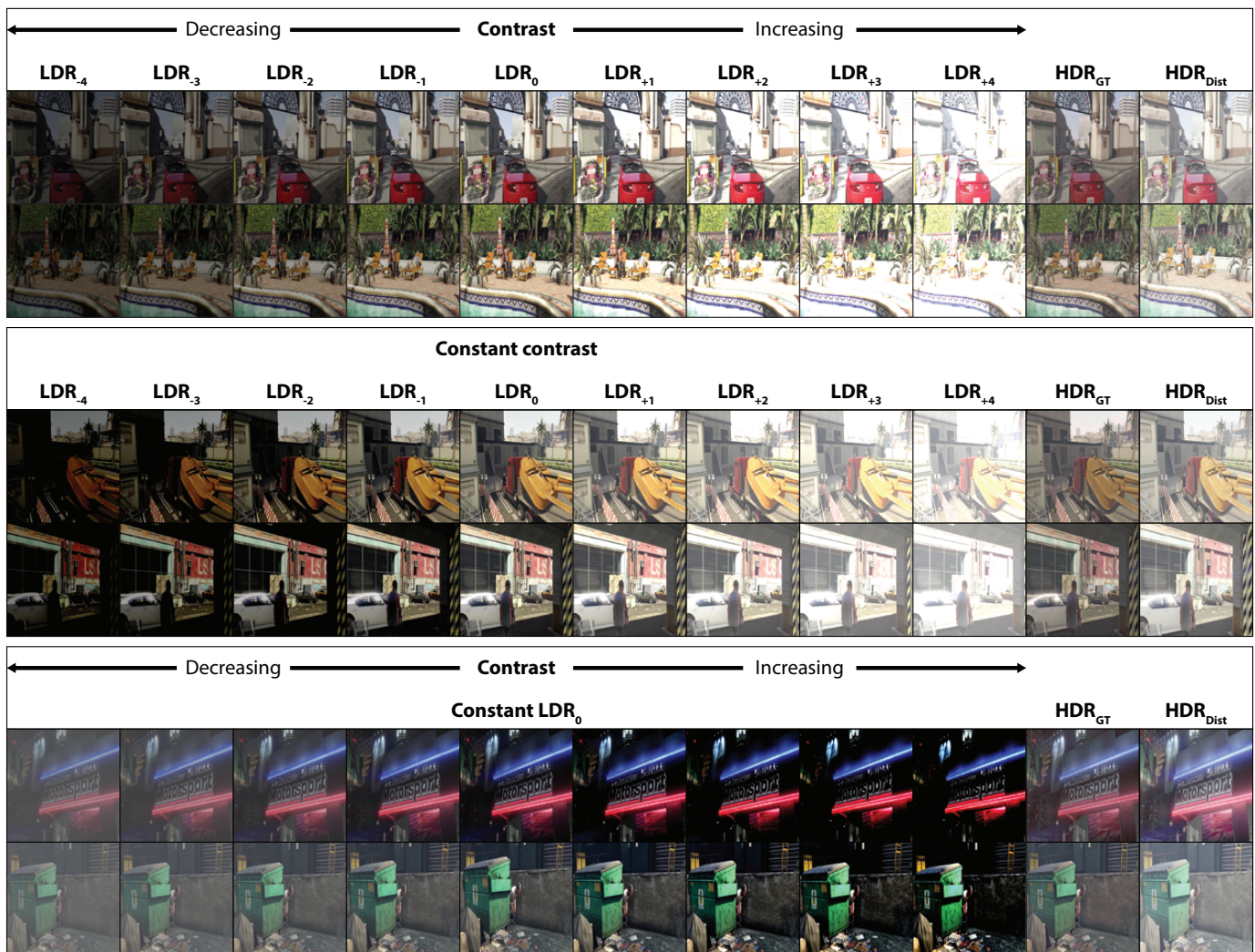


Fig. 3: GTA-HDR dataset image diversity. Samples from GTA-HDR dataset with multiple exposure values, contrast levels and their combinations. For any image-to-image translation dataset, it is important to include a sufficient samples with diverse range of color hues, saturation, exposure, and contrast levels.

also generated 40K distorted HDR images by utilizing the following state-of-the-art methods: [5], [28], [50], [52]; 20K images were generated using [52], 10K with [50], and [5], [28] were used to produce 5K images each.

B. Dataset Characteristics

One of the limitations of existing datasets is the low diversity of scenes and images. To address this limitation, the GTA-HDR dataset includes a wide variety of scenes (*e.g.*, indoor, outdoor, in-the-wild, multiple locations, weather conditions, lighting conditions, and time-of-day) and images (*e.g.*, LDR images with 9 different exposure values EV 0, ± 1 , ± 2 , ± 3 , and ± 4 and contrast levels).

1) Scene Diversity

Real-life scenes can have a wide range of variety in terms of locations, landscapes, objects, humans, animals, buildings, weather, and lighting conditions. Fig. 2 depicts samples from the GTA-HDR dataset with multiple variations in location, weather, objects and time. The diverse set of locations ensures

a thorough coverage of pixel colors, brightness, and luminance. The weather conditions contribute to the rich gamut of brightness levels, *e.g.*, sunny weather scenes will have a larger number of bright pixels than cloudy or rainy scenes. Scenes at different time (*i.e.*, morning, midday, evening, and night) also contribute to different lighting conditions. The diversity of objects not only captures different color hues but also different contrast and saturation levels.

2) Image Diversity

Images can have a diverse range of color hues, saturation, exposure, and contrast levels. For any image-to-image translation dataset, it is important to include a sufficient amount of samples from these categories. Therefore, we introduced different exposure, brightness, and contrast levels in the GTA-HDR dataset. Considering all variations, the dataset includes 24 variants of the original LDR images. The final set of images amounts to a total of $40K \times 25 = 1M$ LDR, 40K HDR, and 40K distorted HDR images. Fig. 3 provides samples from the GTA-HDR dataset with 9 exposure levels (*i.e.*, exposure

values EV 0, ± 1 , ± 2 , ± 3 , and ± 4) and 9 contrast levels of the LDR images. The first two rows show the LDR images with varying contrast and EV levels. The LDR images with normal contrast level are shown in the middle, while LDR images with increasing EV and contrast are shown in sequential order toward the right, and vice versa. On the extreme right, the corresponding HDR and a sample of distorted HDR (*i.e.*, saturation altered HDR) images are illustrated. Here, saturation alteration, contrast alteration, color hue alteration, and noise addition are applied to the HDR to produce the respective distorted HDR images. Similarly, the second and third rows show the LDR images with only varied EV while the contrast is kept constant (*i.e.*, keeping the contrast level of the original LDR image). Finally, in the fifth and sixth rows, the EV is kept constant (*i.e.*, keeping the EV 0 of the original LDR image) and the contrast levels are varied.

3) No-Reference Quality Assessment

To address the data gap for no-reference image quality assessment, the GTA-HDR dataset contributes a set of distorted HDR along with the ground truth HDR and LDR images. The distorted HDR images can be utilized to develop no-reference quality assessment methods, *e.g.*, by adopting a methodology similar to the ones proposed in [34]–[36]: 1) Estimate the full-reference quality scores for pairs of ground truth and distorted HDR images using an existing metric such as PSNR, SSIM, HDR-VDP-2/-3, and LPIPS; 2) Develop a data-driven method using the full-reference quality scores and their corresponding distorted HDR images; and 3) Utilize the developed model to estimate the quality scores of unseen reconstructed HDR images (no-reference quality assessment). Similarly, one can develop data-driven methods to estimate the quality scores for tone-mapped LDR and HDR images.

IV. EXPERIMENTS

We perform a thorough evaluation of the GTA-HDR dataset and assess its contribution to HDR image reconstruction. We further demonstrate the contribution of the proposed dataset by analyzing its impact on three additional computer vision tasks, including 3D human pose estimation, human body part segmentation, and holistic scene segmentation.

A. Experimental Setup

1) Implementation

We used an Ubuntu 20.04.6 LTS workstation with Intel® Xeon® CPU E5-2687W v3 @ 3.10GHz (20 CPU cores), 126 GB RAM (+ 2 GB swap), NVIDIA GeForce GTX 1080 GPU (8 GB memory), and 1.4 TB SSD.

2) Methods

To evaluate the effectiveness of the GTA-HDR dataset, we utilized existing state-of-the-art HDR image reconstruction methods including FHDR [52], SingleHDR [28], [50], HDRCNN [21], HDR-GAN [69], DrTMO [20], ArtHDR-Net [53], and HistoHDR-Net [70]. Most of these methods are designed for single-exposed LDR image inputs, while HDR-GAN is designed for three multi-exposed LDR image inputs, SingleHDR [50] for two or more multi-exposed LDR image

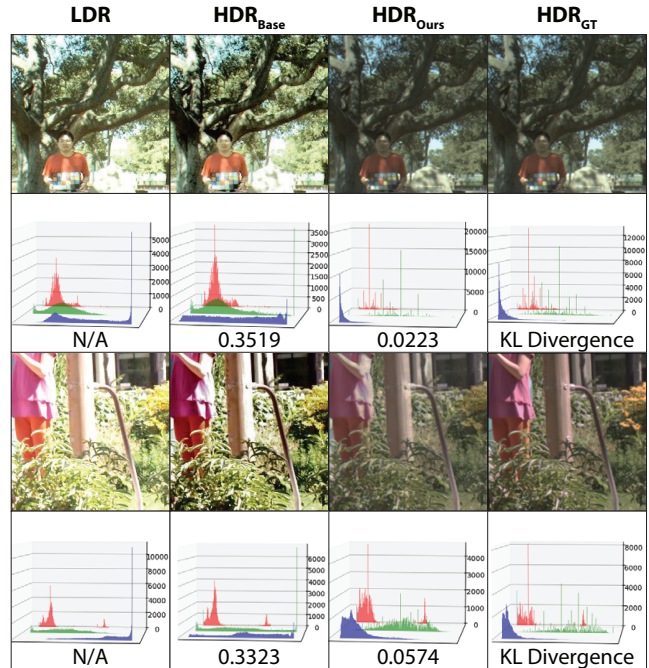


Fig. 4: HDR images reconstructed with and without GTA-HDR as part of the training dataset, along with the RGB histograms and KL-divergence values. *Base*: HDR images reconstructed with ArtHDR-Net [53] trained without GTA-HDR data; *Ours*: HDR images reconstructed with ArtHDR-Net [53] trained with GTA-HDR data; *GT*: Ground truth.

inputs without HDR supervision, and ArtHDR-Net attempts to generate perceptually realistic HDR image using features from multi-exposed LDR images. HistoHDR-Net uses histogram-equalized LDR images along with original LDR images as input to facilitate better recovery of color, contrast, saturation, and hue from over/under-exposed regions.

Unless specified otherwise, we used the official implementations and training strategies of the existing state-of-the-art HDR image reconstruction methods. Since, SingleHDR [50] generates multi-exposed LDR images as output, we used the state-of-the-art tool Photomatrix [71] to merge the LDR stack to obtain and HDR image. For single-exposed LDR image input methods, we consider all of the available LDR images in the datasets. For multi-exposed LDR image inputs: 1) For methods with three inputs, we consider an overexposed, a normally exposed, and an underexposed LDR image; and 2) For methods with two inputs, we consider an overexposed and an underexposed LDR image. For existing datasets with single-exposed LDR images, we generated the missing exposure variants. The diversity of the considered approaches enables a thorough and all-round evaluation of the proposed GTA-HDR dataset.

3) Datasets

We considered most publicly available datasets for HDR image reconstruction in our experiments [19], [24]–[28]. We split the data into a training set consisting of the datasets proposed in [19], [24]–[27] and test set including the dataset proposed in [28]. We considered different datasets for train-

TABLE II: **Impact of the GTA-HDR dataset on the performance of the state-of-the-art in HDR image reconstruction.** *R*: Real data combines the datasets proposed in [19], [24], [25] and the real images from the datasets proposed in [26], [27]; $R \oplus S$: This combination contains the mixed datasets (including both real and synthetic data) proposed in [26], [27] and the real datasets proposed in [19], [24], [25]; *GTA-HDR*: Proposed synthetic dataset; *E2E*: End-to-end training; *FT*: Finetuning of the original pre-trained models. The performance of all methods is evaluated on a separate dataset proposed in [28].

Method	Configuration	Datasets	PSNR \uparrow	SSIM \uparrow	Q-score \uparrow
HDRCNN [21]	E2E	R	19.1	0.67	59.2
DrTMO [20]	E2E	R	19.2	0.68	60.3
FHDR [52]	E2E	R	24.4	0.80	65.1
SingleHDR [28]	E2E	R	29.1	0.81	66.2
HDR-GAN [69]	E2E	R	36.9	0.92	65.3
SingleHDR [50]	E2E	R	34.7	0.91	66.9
ArtHDR-Net [53]	E2E	R	35.1	0.91	67.2
HistoHDR-Net [70]	E2E	R	35.2	0.92	67.4
<hr/>					
HDRCNN [21]	E2E	$R \oplus S$	20.1	0.69	60.8
DrTMO [20]	E2E	$R \oplus S$	20.3	0.68	61.5
FHDR [52]	E2E	$R \oplus S$	26.7	0.81	65.3
SingleHDR [28]	E2E	$R \oplus S$	30.4	0.82	66.1
HDR-GAN [69]	E2E	$R \oplus S$	37.8	0.94	66.7
SingleHDR [50]	E2E	$R \oplus S$	35.2	0.92	67.1
ArtHDR-Net [53]	E2E	$R \oplus S$	35.3	0.93	67.4
HistoHDR-Net [70]	E2E	$R \oplus S$	35.3	0.94	67.5
<hr/>					
HDRCNN [21]	E2E / FT	GTA-HDR	22.4 / 22.1	0.72 / 0.71	61.3 / 61.4
DrTMO [20]	E2E / FT	GTA-HDR	23.5 / 23.4	0.71 / 0.71	64.3 / 64.5
FHDR [52]	E2E / FT	GTA-HDR	27.7 / 27.6	0.84 / 0.84	68.0 / 68.1
SingleHDR [28]	E2E / FT	GTA-HDR	32.3 / 32.1	0.86 / 0.85	68.8 / 69.0
HDR-GAN [69]	E2E / FT	GTA-HDR	38.7 / 38.5	0.94 / 0.93	69.5 / 69.7
SingleHDR [50]	E2E / FT	GTA-HDR	41.2 / 41.5	0.96 / 0.96	70.2 / 70.0
ArtHDR-Net [53]	E2E / FT	GTA-HDR	41.6 / 41.5	0.97 / 0.97	70.4 / 70.2
HistoHDR-Net [70]	E2E / FT	GTA-HDR	41.7 / 41.5	0.98 / 0.98	70.5 / 70.4
<hr/>					
HDRCNN [21]	E2E / FT	$R \oplus S \oplus$ GTA-HDR	22.6 (+3.5) / 22.3 (+3.2)	0.70 (+0.03) / 0.69 (+0.02)	61.6 (+2.4) / 62.0 (+2.8)
DrTMO [20]	E2E / FT	$R \oplus S \oplus$ GTA-HDR	23.6 (+4.4) / 23.5 (+4.3)	0.71 (+0.03) / 0.72 (+0.04)	64.6 (+4.3) / 64.8 (+4.5)
FHDR [52]	E2E / FT	$R \oplus S \oplus$ GTA-HDR	27.9 (+3.5) / 27.4 (+3.0)	0.83 (+0.03) / 0.83 (+0.03)	67.5 (+2.4) / 68.1 (+3.0)
SingleHDR [28]	E2E / FT	$R \oplus S \oplus$ GTA-HDR	32.5 (+3.4) / 31.6 (+2.5)	0.85 (+0.04) / 0.84 (+0.03)	68.7 (+2.5) / 68.8 (+2.6)
HDR-GAN [69]	E2E / FT	$R \oplus S \oplus$ GTA-HDR	40.1 (+3.2) / 39.4 (+2.5)	0.95 (+0.03) / 0.97 (+0.05)	69.2 (+3.9) / 69.5 (+4.2)
SingleHDR [50]	E2E / FT	$R \oplus S \oplus$ GTA-HDR	41.5 (+6.8) / 41.9 (+7.2)	0.97 (+0.06) / 0.98 (+0.07)	70.3 (+3.4) / 70.0 (+3.1)
ArtHDR-Net [53]	E2E / FT	$R \oplus S \oplus$ GTA-HDR	41.6 (+6.5) / 42.1 (+7.0)	0.98 (+0.07) / 0.98 (+0.07)	71.2 (+4.0) / 70.9 (+3.7)
HistoHDR-Net [70]	E2E / FT	$R \oplus S \oplus$ GTA-HDR	41.8 (+6.6) / 42.3 (+7.1)	0.99 (+0.07) / 0.99 (+0.07)	71.5 (+4.1) / 71.4 (+4.0)

ing and testing to demonstrate that GTA-HDR both enables significant improvements in the quality of the reconstructed HDR images and contributes towards better generalization capabilities of the considered state-of-the-art HDR image reconstruction methods. Unless specified otherwise, the same protocol for training and testing was used in all experiments to ensure a fair comparison. All images were resized to 512×512 resolution before being used for training and testing. All HDR images displayed in this text have been tone-mapped using the method proposed in [72].

B. Evaluation Metrics

We used three metrics to report the quantitative results. *High Dynamic Range Visual Differences Predictor* (HDR-VDP-2) [73] or Q-Score (Mean Opinion Score Index) is used for evaluation based on the human visual system. For structural similarity, luminance, and contrast comparisons, the *Structural Similarity Index Measure* (SSIM) [74]–[76] is used. For pixel-to-pixel comparisons, the *Peak Signal-to-Noise Ratio* (PSNR) [77] is applied.⁷

⁷Unless specified otherwise, PSNR is computed on tone-mapped original and reconstructed HDR image pairs.

V. RESULTS

A. HDR Image Reconstruction

This section presents the results from state-of-the-art HDR image reconstruction methods trained with different configurations of data, including real data, mixed data, and synthetic data. The results are based on two training strategies chosen to evaluate the contributions of the proposed GTA-HDR dataset: 1) End-to-end training (*i.e.*, the models are fully trained with different combinations of data as stated in Section IV-A3), and 2) Finetuning (*i.e.*, only the final layers of the pre-trained original models are trained with different combinations of data). The quantitative results of this experiment are summarized in Table II. The results show a consistent improvement in PSNR, SSIM, and HDR-VDP-2 (Q-score) for all methods, after including the GTA-HDR dataset in the training process. Furthermore, the results also demonstrate that all the considered state-of-the-art methods trained with GTA-HDR data alone achieved better performance than when they are trained with existing real and synthetic datasets (see third sub-table). Moreover, Table II shows how the performance of the state-of-the-art methods improve consistently when we add more variations to the training data, starting with real data in first sub-table and eventually the full mixture of real,

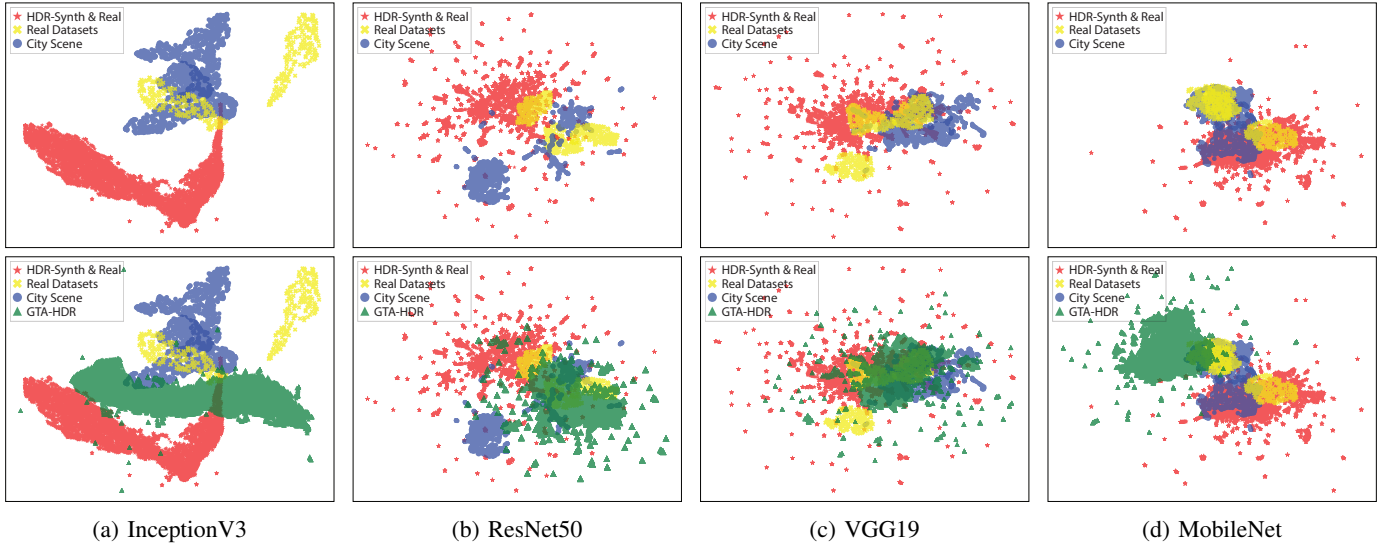


Fig. 5: **Feature space covered by different conventional HDR image reconstruction datasets.** We used UMAP [78] dimension reduction technique to visualize the features extracted from the most common pre-trained feature extraction backbones. *Real Datasets*: Real data combines the datasets proposed in [19], [24], [25]; *City Scene*: Mixed datasets proposed in [26], [27]; *HDR-Synth & HDR-Real*: Mixed dataset proposed in [28]; *GTA-HDR*: Proposed synthetic dataset.

synthetic, and GTA-HDR in the last sub-table. We also observe that adding variation to data leads to better results from the second sub-table which has a combination of existing real and synthetic datasets. Further improvements are achieved when mixing the existing datasets with GTA-HDR in both end-to-end and fine-tuning strategies. It is noteworthy that methods such as FHDR [52] trained with GTA-HDR data using both end-to-end and fine-tuning strategies perform better than some of the more complicated newer methods, *e.g.*, SingleHDR [28], [50] and HDR-GAN [69] in terms of HDR-VDP-2 (Q-score) and SSIM.

Fig. 4 illustrates examples of HDR images reconstructed by training [53] with the GTA-HDR data in an end-to-end fashion. The histograms of the ground truth and the reconstructed images are also included. We can see that the histograms from the method trained with GTA-HDR data (*i.e.*, HDR_{Ours}) are more similar to the histograms of ground truth HDR images (*i.e.*, HDR_{GT}) than those from the method trained without GTA-HDR data (*i.e.*, HDR_{Base}). We also report the Kullback-Leibler (KL) divergence values for tone-mapped HDR_{GT} and tone-mapped HDR_{Base} and HDR_{Ours} using the RGB intensities. We see the average KL divergence of the RGB histogram intensity distributions are significantly lower for HDR_{Ours} compared to HDR_{Base}. Further results are provided in the Supplementary Material.

B. Scene Diversity

In this experiment, we study the feature space coverage of different datasets as reported by common feature extraction backbones including MobileNet [79], InceptionV3 [80], ResNet50 [62], and VGG19 [81]. The results reveal a gap in the feature space, *i.e.*, certain regions are not covered by existing real and mixed datasets. These regions are filled, to a certain extent, by the proposed GTA-HDR dataset. Features extracted from different backbones can be significantly

TABLE III: **Performance of SingleHDR [50].** Different versions of the state-of-the-art method utilizing different feature extraction backbones, trained with and without GTA-HDR data in an end-to-end fashion. $R \oplus S$: Contains the mixed datasets (including both real and synthetic data) proposed in [26], [27] and the real datasets proposed in [19], [24], [25]; *GTA-HDR*: Proposed synthetic dataset. All versions of SingleHDR [50] are evaluated on a separate dataset proposed in [28].

Method	#Param	Datasets (training)	PSNR \uparrow	SSIM \uparrow
SingleHDR (MobileNet)	13M	$R \oplus S$	32.3	0.89
SingleHDR (InceptionV3)	24M	$R \oplus S$	32.8	0.89
SingleHDR (ResNet50)	25.6M	$R \oplus S$	33.2	0.90
SingleHDR (VGG19)	144M	$R \oplus S$	35.2	0.92
SingleHDR (MobileNet)	13M	GTA-HDR	38.4	0.94
SingleHDR (InceptionV3)	24M	GTA-HDR	38.8	0.95
SingleHDR (ResNet50)	25.6M	GTA-HDR	39.5	0.95
SingleHDR (VGG19)	144M	GTA-HDR	41.2	0.96
SingleHDR (MobileNet)	13M	$R \oplus S \oplus$ GTA-HDR	38.6 (+6.3)	0.95 (+0.06)
SingleHDR (InceptionV3)	24M	$R \oplus S \oplus$ GTA-HDR	39.5 (+6.7)	0.95 (+0.06)
SingleHDR (ResNet50)	25.6M	$R \oplus S \oplus$ GTA-HDR	40.1 (+6.9)	0.96 (+0.06)
SingleHDR (VGG19)	144M	$R \oplus S \oplus$ GTA-HDR	41.5 (+6.3)	0.97 (+0.05)

different based on the underlying architecture, which affects the performance on the downstream tasks (*e.g.*, HDR image reconstruction). The main goal of feature extraction backbones in LDR to HDR image conversion is the recognition of bright and dark regions and detection of the light source [62] to ensure that underexposed and overexposed regions are treated separately. Fig. 5 illustrates the feature plots for different datasets. The first column shows the output of InceptionV3 on existing datasets (top) and the GTA-HDR dataset included (bottom). There is a significant gap in the feature space between the HDR-Synth & Real dataset (red) and City Scene dataset (blue) as well as real datasets combined (yellow), which is filled, to some extent, by the GTA-HDR dataset

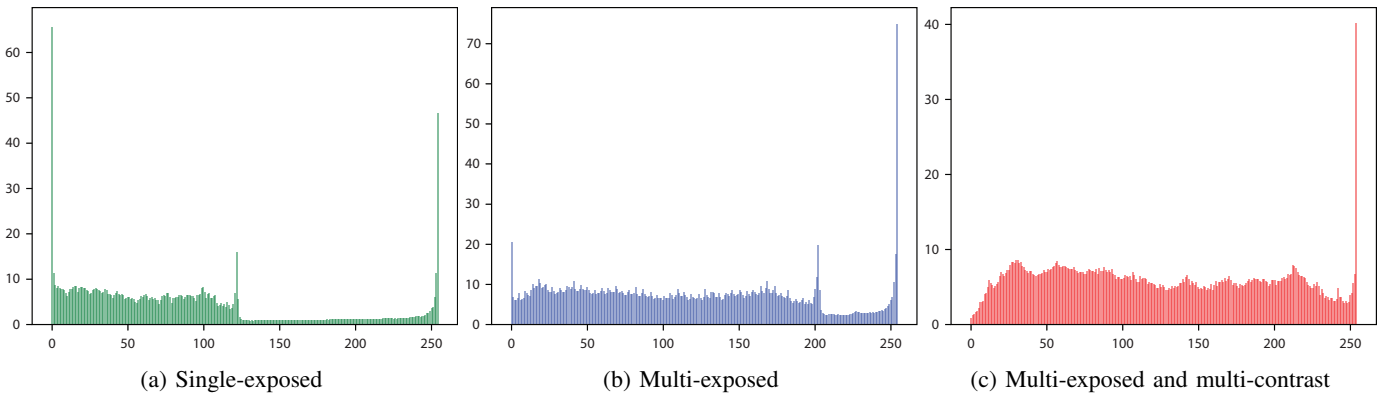


Fig. 6: **Histograms of different variants of the GTA-HDR dataset.** a) $\text{GTA-HDR}_{\text{SE}}$ with only single-exposed LDR images, b) $\text{GTA-HDR}_{\text{ME}}$ with only multi-exposed LDR images, and c) $\text{GTA-HDR}_{\text{FULL}}$ with all LDR images.

(green). In the second column (ResNet50), GTA-HDR fills the gap in the lower right corner of the feature space. Here, we also observed a significant overlap of the GTA-HDR dataset with other datasets. In the third column (VGG19), the GTA-HDR dataset alone covers a significant area of the feature space which is covered by all other datasets combined. Finally, in the last column (MobileNet), GTA-HDR extends the feature space by covering a considerable area of the upper left corner along with some overlap with the existing datasets.

To further investigate the contribution of the GTA-HDR dataset, we replaced the feature extraction block of one of the most recent state-of-the-art methods, SingleHDR [50] (which originally utilizes VGG19), with the described feature extraction backbones. Table III summarizes the quantitative results of this experiment in terms of PSNR and SSIM. When the model is trained with existing real and mixed datasets in an end-to-end fashion, the observed improvements are proportional to the size of the backbones (*i.e.*, the number of parameters). However, using only GTA-HDR data for training, there is a significant improvement for all the backbones. It is worth noting that regardless of the size of the backbone feature extractor, there is an improvement in both PSNR and SSIM when using GTA-HDR. Interestingly, when including the GTA-HDR dataset, the performance of the considerably smaller (*e.g.*, MobileNet) backbones is better than the large ones (*e.g.*, VGG19) trained without using GTA-HDR.

C. Image Diversity

The existing datasets include either single-exposed or multi-exposed LDR images and the corresponding HDR images. The GTA-HDR dataset also introduces LDR images with multi-contrast levels for each HDR image. In this section, we report the results of an experiment that aims to establish the contribution of multi-exposed and multi-contrast LDR images on the HDR image reconstruction performance. The experiment includes 3 versions of the GTA-HDR dataset: 1) $\text{GTA-HDR}_{\text{SE}}$ consists of only single-exposed LDR images; 2) $\text{GTA-HDR}_{\text{ME}}$ comprises only multi-exposed LDR images; and 3) $\text{GTA-HDR}_{\text{FULL}}$ includes all LDR images (*i.e.*, multi-exposed and multi-contrast). Fig. 6 illustrates the histograms of the three versions of the dataset. We treat RGB channels each

TABLE IV: **Performance of ArtHDR-Net [53].** Assessment of the state-of-the-art method utilizing different training and testing datasets. *SE*: GTA-HDR without exposure and contrast variations; *ME*: GTA-HDR with different exposure levels; *FULL*: Proposed synthetic dataset; *U*: Underexposed LDR images; *O*: Overexposed LDR images; *N*: Normally exposed LDR images. All versions of ArtHDR-Net [53] are evaluated on a separate dataset proposed in [28].

Datasets (training)	Datasets (testing)	PSNR \uparrow	SSIM \uparrow	Q-score \uparrow
$\text{GTA-HDR}_{\text{SE}}$	U	42.9	0.99	73.3
$\text{GTA-HDR}_{\text{ME}}$	U	40.7	0.97	71.2
$\text{GTA-HDR}_{\text{FULL}}$	U	39.1	0.95	69.4
$\text{GTA-HDR}_{\text{SE}}$	O	32.8	0.89	64.9
$\text{GTA-HDR}_{\text{ME}}$	O	33.9	0.92	65.7
$\text{GTA-HDR}_{\text{FULL}}$	O	34.7	0.93	66.4
$\text{GTA-HDR}_{\text{SE}}$	U + O + N	37.2	0.93	66.2
$\text{GTA-HDR}_{\text{ME}}$	U + O + N	39.7	0.95	68.5
$\text{GTA-HDR}_{\text{FULL}}$	U + O + N	41.6	0.97	70.4

as intensity values without any conversion. The histogram for $\text{GTA-HDR}_{\text{SE}}$ reveals that there is a miss-balance in the dataset, where most image pixel intensity values are on the left-hand side of the histogram (*i.e.*, under-exposed pixels [0, 150]). The histogram for $\text{GTA-HDR}_{\text{ME}}$ demonstrates that a portion of the miss-balance has been addressed (with a small gap in the interval [200, 250]). The histogram for $\text{GTA-HDR}_{\text{FULL}}$ confirms that the intensity values are more evenly distributed.

Table IV summarizes the quantitative results of this analysis. In this experiment, we consider the recent state-of-the-art method ArtHDR-Net [53]. The first three rows report the performance of ArtHDR-Net trained with each version of the GTA-HDR dataset and tested on reconstructing HDR images from underexposed LDR images. The performance of the model trained with $\text{GTA-HDR}_{\text{SE}}$ dataset is surprisingly good in the case of underexposed LDR images, supporting the qualitative results from the left histogram in Fig. 6. The middle three rows report the performance of ArtHDR-Net trained with each version of the GTA-HDR dataset and tested on reconstructing HDR images from overexposed LDR images. In this case, the performance steadily increases with the addition of exposure and contrast levels in the training set.

TABLE V: **Impact of the GTA-HDR dataset on the performance of the state-of-the-art in 3D human pose and shape estimation, 2D human body part segmentation, and semantic segmentation.** We used ArtHDR-Net [53] trained with different datasets for HDR image reconstruction. The resulting HDR images from 1) AGORA [83] 3D human pose dataset were used by BEV [82] for 3D human pose and shape estimation; 2) COCO-DensePose [84] dataset were used by CDCL [85] for 2D human body part segmentation; and 3) Cityscapes [86] dataset were used by SAM [87] for semantic segmentation. $R \oplus S$: This combination contains the mixed datasets (including both real and synthetic data) proposed in [26], [27] and the real datasets proposed in [19], [24], [25]; *GTA-HDR*: Proposed synthetic dataset; *None*: Results without HDR image reconstruction.

Pre-processing	Datasets	3D human pose and shape estimation		2D human body part segmentation	Semantic segmentation
		F1 (detection) \uparrow	MPJPE (pose) \downarrow	mIOU% \uparrow	mIOU% \uparrow
None	-	0.57	129	66.24	54.24
ArtHDR-Net	-	0.58	128.7	67.12	54.27
ArtHDR-Net	$R \oplus S$	0.58	128.5	67.9	54.26
ArtHDR-Net	GTA-HDR	0.61	125.4	69.55	54.29
ArtHDR-Net	$R \oplus S \oplus$ GTA-HDR	0.65	121.9	74.71	54.36

A similar trend can be observed on the combined over- and underexposed LDR images, reported in the bottom three rows. Images of real-life scenes have diverse exposure and contrast levels suggesting a data distribution similar to the proposed GTA-HDR_{FULL} dataset. In addition, multi-exposed and multi-contrast LDR images help mitigate model bias towards certain classes of images. Further qualitative results are provided in the Supplementary Material.

D. Downstream Applications

To further demonstrate the contribution of the proposed GTA-HDR dataset, this section illustrates its impact on the state-of-the-art in other computer vision tasks including 3D human pose estimation, human body part segmentation, and holistic scene segmentation. Qualitative results for all three tasks are provided in the Supplementary Material.

1) 3D Human Pose and Shape Estimation

We used BEV [82] as a state-of-the-art pre-trained 3D human pose and shape estimator from images. We tested the BEV model on the reconstructed HDR images from several versions of the state-of-the-art method ArtHDR-Net [53]. Table V reports the impact of the image pre-processing step (utilizing reconstructed HDR images from different versions of ArtHDR-Net) on BEV performance evaluated on the AGORA [83] 3D human pose dataset. We report two commonly used metrics, *F1 Score* to measure detection accuracy and *Mean Per Joint Position Error* (MPJPE) to measure pose accuracy. The results demonstrate that the pre-processing step enables a significant increase in the performance of BEV.

2) Human Body Part Segmentation

In this experiment, we used CDCL [85], a state-of-the-art body part segmentation model. Similar to the previous case, we tested the model on reconstructed HDR images from several versions of ArtHDR-Net [53]. Table V reports the impact of the HDR reconstruction step on the COCO-DensePose [84] dataset, which is used for CDCL performance evaluation. We use the *Mean Intersection of Union* (mIOU%), *i.e.*, the mean of all IoUs between predicted and ground truth masks to measure the accuracy of the predictions. We report the average accuracy for all the body parts considered in [85]. The results establish

the advantages of using the proposed pre-processing (*i.e.*, HDR reconstruction) step.

3) Semantic Segmentation

Finally, we report an experiment on another vision application, *i.e.*, holistic semantic segmentation of scenes, which is an important task in robotics and human-robot interaction. We consider a recent state-of-the-art method called SAM [87] as a pre-trained holistic scene segmentation model. Table V reports the improvements in the SAM output using the HDR reconstruction as a pre-processing step with the Cityscapes [86] dataset. We use *Mean Intersection of Union* (mIOU%) as the accuracy measure for segmentation. The results show steady improvements in the performance of SAM.

VI. CONCLUSIONS

This work proposes GTA-HDR, a novel large-scale synthetic dataset and data collection pipeline to complement existing real and synthetic datasets for HDR image reconstruction. The thorough experimental validation using existing real and synthetic datasets and state-of-the-art methods highlights the contribution of the proposed dataset, specifically to the quality of HDR image reconstruction and the recovery of image details with high fidelity. We further demonstrate the contribution of the proposed dataset by illustrating its impact on the state-of-the-art in other computer vision tasks, including 3D human pose estimation, human body part segmentation, and holistic scene segmentation. The proposed dataset represents an important contribution that will enable the development of advanced techniques for visually accurate HDR image reconstruction. Preliminary discussion has been presented for developing no-reference quality assessment methods utilising the GTA-HDR dataset. This is possible direction for future research in addition to creating a video-based HDR reconstruction dataset.

COPYRIGHT

As per the publisher's policy⁸ for the GTA-V game⁹, it allows the use of the generated game-play data provided it is used for non-commercial purposes and without any spoilers.

⁸Policy on copyrighted material: <http://tinyurl.com/pjfoqo5>

⁹Policy on mods: <http://tinyurl.com/yc8kq7vn>

REFERENCES

- [1] A. Artusi, R. K. Mantiuk, T. Richter, P. Hanhart, P. Korshunov, M. Agostinelli, A. Ten, and T. Ebrahimi, "Overview and evaluation of the JPEG XT HDR image compression standard," *Journal of Real-Time Image Processing*, vol. 16, pp. 413–428, 2019.
- [2] G. He, K. Xu, L. Xu, C. Wu, M. Sun, X. Wen, and Y.-W. Tai, "SDRTV-to-HDRTV via Hierarchical Dynamic Context Feature Mapping," in *Proceedings of the 30th ACM International Conference on Multimedia*, 2022, pp. 2890–2898.
- [3] P. Satilmis and T. Bashford-Rogers, "Deep Dynamic Cloud Lighting," *arXiv preprint arXiv:2304.09317*, 2023.
- [4] X. Huang, Q. Zhang, Y. Feng, H. Li, X. Wang, and Q. Wang, "HDR-NeRF: High Dynamic Range Neural Radiance Fields," in *Proceedings of the IEEE/CVF Conference on Computer Vision and Pattern Recognition*, 2022, pp. 18 398–18 408.
- [5] H. Nguyen, D. Tran, K. Nguyen, and R. Nguyen, "PSENet: Progressive Self-Enhancement Network for Unsupervised Extreme-Light Image Enhancement," in *Proceedings of the IEEE/CVF Winter Conference on Applications of Computer Vision*, 2023, pp. 1756–1765.
- [6] X. Wu, H. Zhang, X. Hu, M. Shakeri, C. Fan, and J. Ting, "HDR reconstruction based on the polarization camera," *IEEE Robotics and Automation Letters*, vol. 5, no. 4, pp. 5113–5119, 2020.
- [7] L. Wang and K.-J. Yoon, "Deep Learning for HDR Imaging: State-of-the-Art and Future Trends," *IEEE transactions on pattern analysis and machine intelligence*, vol. 44, no. 12, pp. 8874–8895, 2021.
- [8] G. Tiwari and P. Rani, "A Review On High-Dynamic-Range Imaging With Its Technique," *International Journal of Signal Processing, Image Processing and Pattern Recognition*, vol. 8, no. 9, pp. 93–100, 2015.
- [9] O. T. Tursun, A. O. Akyüz, A. Erdem, and E. Erdem, "The State of the Art in HDR Deghosting: A Survey and Evaluation," in *Computer Graphics Forum*, vol. 34, no. 2. Wiley Online Library, 2015, pp. 683–707.
- [10] A. K. Johnson, "High Dynamic Range Imaging - A Review," *Int. J. Image Process.(IJIP)*, vol. 9, p. 198, 2015.
- [11] H. Wang, M. Ye, X. Zhu, S. Li, C. Zhu, and X. Li, "KUNet: Imaging Knowledge-Inspired Single HDR Image Reconstruction," in *The 31st International Joint Conference On Artificial Intelligence (IJCAI/ECAI 22)*, 2022.
- [12] Y. Kinoshita and H. Kiya, "Scene segmentation-based luminance adjustment for multi-exposure image fusion," *IEEE Transactions on Image Processing*, vol. 28, no. 8, pp. 4101–4116, 2019.
- [13] G. Luzardo, J. Aelterman, H. Luong, W. Philips, D. Ochoa, and S. Rousseaux, "Fully-Automatic Inverse Tone Mapping Preserving the Content Creator's Artistic Intentions," in *2018 Picture Coding Symposium (PCS)*. IEEE, 2018, pp. 199–203.
- [14] R. P. Kovaleski and M. M. Oliveira, "High-Quality Reverse Tone Mapping for a Wide Range of Exposures," in *2014 27th SIBGRAPI Conference on Graphics, Patterns and Images*. IEEE, 2014, pp. 49–56.
- [15] Y. Huo, F. Yang, L. Dong, and V. Brost, "Physiological inverse tone mapping based on retina response," *The Visual Computer*, vol. 30, pp. 507–517, 2014.
- [16] B. Masia, A. Serrano, and D. Gutierrez, "Dynamic range expansion based on image statistics," *Multimedia Tools and Applications*, vol. 76, pp. 631–648, 2017.
- [17] B.-C. Guo and C.-H. Lin, "Single-Image HDR Reconstruction Based on Two-Stage GAN Structure," in *2023 IEEE International Conference on Image Processing (ICIP)*. IEEE, 2023, pp. 91–95.
- [18] D. Dalal, G. Vashishtha, P. Singh, and S. Raman, "Single Image LDR to HDR Conversion Using Conditional Diffusion," in *2023 IEEE International Conference on Image Processing (ICIP)*. IEEE, 2023, pp. 3533–3537.
- [19] N. K. Kalantari, R. Ramamoorthi *et al.*, "Deep High Dynamic Range Imaging of Dynamic Scenes," *ACM Trans. Graph.*, vol. 36, no. 4, pp. 144–1, 2017.
- [20] Y. Endo, Y. Kanamori, and J. Mitani, "Deep reverse tone mapping," *ACM Trans. Graph.*, vol. 36, no. 6, pp. 177–1, 2017.
- [21] G. Eilertsen, J. Kronander, G. Denes, R. K. Mantiuk, and J. Unger, "HDR image reconstruction from a single exposure using deep CNNs," *ACM transactions on graphics (TOG)*, vol. 36, no. 6, pp. 1–15, 2017.
- [22] H. Nemoto, P. Korshunov, P. Hanhart, and T. Ebrahimi, "Visual attention in LDR and HDR images," in *9th International Workshop on Video Processing and Quality Metrics for Consumer Electronics (VPQM)*, no. CONF, 2015.
- [23] S. Lee, G. H. An, and S.-J. Kang, "Deep Chain HDRI: Reconstructing a High Dynamic Range Image from a Single Low Dynamic Range Image," *IEEE Access*, vol. 6, pp. 49 913–49 924, 2018.
- [24] K. R. Prabhakar, R. Arora, A. Swaminathan, K. P. Singh, and R. V. Babu, "A Fast, Scalable, and Reliable Deghosting Method for Extreme Exposure Fusion," in *2019 IEEE International Conference on Computational Photography (ICCP)*. IEEE, 2019, pp. 1–8.
- [25] H. Jang, K. Bang, J. Jang, and D. Hwang, "Dynamic Range Expansion Using Cumulative Histogram Learning for High Dynamic Range Image Generation," *IEEE Access*, vol. 8, pp. 38 554–38 567, 2020.
- [26] J. Zhang and J.-F. Lalonde, "Learning High Dynamic Range from Outdoor Panoramas," in *Proceedings of the IEEE International Conference on Computer Vision*, 2017, pp. 4519–4528.
- [27] L. et al., "The Laval HDR sky database," <http://hdrdb.com/>, 2016, [Online; accessed 3-July-2023].
- [28] Y.-L. Liu, W.-S. Lai, Y.-S. Chen, Y.-L. Kao, M.-H. Yang, Y.-Y. Chuang, and J.-B. Huang, "Single-Image HDR Reconstruction by Learning to Reverse the Camera Pipeline," in *Proceedings of the IEEE/CVF Conference on Computer Vision and Pattern Recognition*, 2020, pp. 1651–1660.
- [29] J. Cai, S. Gu, and L. Zhang, "Learning a Deep Single Image Contrast Enhancer from Multi-Exposure Images," *IEEE Transactions on Image Processing*, vol. 27, no. 4, pp. 2049–2062, 2018.
- [30] S. Y. Kim, J. Oh, and M. Kim, "Deep SR-ITM: Joint Learning of Super-Resolution and Inverse Tone-Mapping for 4K UHD HDR Applications," in *Proceedings of the IEEE/CVF international conference on computer vision*, 2019, pp. 3116–3125.
- [31] P. Sen, N. K. Kalantari, M. Yaesoubi, S. Darabi, D. B. Goldman, and E. Shechtman, "Robust Patch-Based HDR Reconstruction of Dynamic Scenes," *ACM Trans. Graph.*, vol. 31, no. 6, pp. 203–1, 2012.
- [32] O. T. Tursun, A. O. Akyüz, A. Erdem, and E. Erdem, "An Objective Deghosting Quality Metric for HDR Images," in *Computer Graphics Forum*, vol. 35, no. 2. Wiley Online Library, 2016, pp. 139–152.
- [33] D.-T. Dang-Nguyen, C. Pasquini, V. Conotter, and G. Boato, "RAISE: A Raw Images Dataset for Digital Image Forensics," in *Proceedings of the 6th ACM multimedia systems conference*, 2015, pp. 219–224.
- [34] F. Banterle, A. Artusi, A. Moreo, and F. Carrara, "Nor-Vdpnet: A No-Reference High Dynamic Range Quality Metric Trained On Hdr-Vdp 2," in *2020 IEEE International Conference on Image Processing (ICIP)*. IEEE, 2020, pp. 126–130.
- [35] F. Banterle, A. Artusi, A. Moreo, F. Carrara, and P. Cignoni, "NoR-VDPNet++: Real-Time No-Reference Image Quality Metrics," *IEEE Access*, vol. 11, pp. 34 544–34 553, 2023.
- [36] A. Artusi, F. Banterle, F. Carra, and A. Moreno, "Efficient Evaluation of Image Quality via Deep-Learning Approximation of Perceptual Metrics," *IEEE Transactions on Image Processing*, vol. 29, pp. 1843–1855, 2019.
- [37] L. Zhang, A. Zhu, S. Zhao, and Y. Zhou, "Simulation of Atmospheric Visibility Impairment," *IEEE Transactions on Image Processing*, vol. 30, pp. 8713–8726, 2021.
- [38] Z. Yang, Z. Cai, H. Mei, S. Liu, Z. Chen, W. Xiao, Y. Wei, Z. Qing, C. Wei, B. Dai *et al.*, "SynBody: Synthetic Dataset with Layered Human Models for 3D Human Perception and Modeling," *arXiv preprint arXiv:2303.17368*, 2023.
- [39] M. Angus, M. ElBalkini, S. Khan, A. Harakeh, O. Andrienko, C. Reading, S. Waslander, and K. Czarniecki, "Unlimited Road-scene Synthetic Annotation (URSA) Dataset," in *2018 21st International Conference on Intelligent Transportation Systems (ITSC)*. IEEE, 2018, pp. 985–992.
- [40] S. R. Richter, Z. Hayder, and V. Koltun, "Playing for Benchmarks," in *Proceedings of the IEEE International Conference on Computer Vision*, 2017, pp. 2213–2222.
- [41] M. Fabbri, G. Brasó, G. Maugeri, O. Cetintas, R. Gasparini, A. Oşep, S. Calderara, L. Leal-Taixé, and R. Cucchiara, "MOTSynth: How Can Synthetic Data Help Pedestrian Detection and Tracking?" in *Proceedings of the IEEE/CVF International Conference on Computer Vision*, 2021, pp. 10 849–10 859.
- [42] Y.-T. Hu, J. Wang, R. A. Yeh, and A. G. Schwing, "SAIL-VOS 3D: A Synthetic Dataset and Baselines for Object Detection and 3D Mesh Reconstruction from Video Data," in *Proceedings of the IEEE/CVF Conference on Computer Vision and Pattern Recognition*, 2021, pp. 1418–1428.
- [43] P. Krähenbühl, "Free Supervision From Video Games," in *Proceedings of the IEEE conference on computer vision and pattern recognition*, 2018, pp. 2955–2964.
- [44] S. R. Richter, V. Vineet, S. Roth, and V. Koltun, "Playing for Data: Ground Truth from Computer Games," in *Computer Vision—ECCV 2016*:

- 14th European Conference, Amsterdam, The Netherlands, October 11-14, 2016, *Proceedings, Part II 14*. Springer, 2016, pp. 102–118.
- [45] C. P. RED, “The Witcher 3: Wild Hunt,” <https://www.thewitcher.com/en/en/witcher3>, 2016, [Online; accessed 3-Dec-2023].
- [46] H. Xu, Y. Gao, F. Yu, and T. Darrell, “End-to-end Learning of Driving Models from Large-scale Video Datasets,” in *Proceedings of the IEEE conference on computer vision and pattern recognition*, 2017, pp. 2174–2182.
- [47] P. Hanji, R. Mantiuk, G. Eilertsen, S. Hajisharif, and J. Unger, “Comparison of single image HDR reconstruction methods—the caveats of quality assessment,” in *ACM SIGGRAPH 2022 conference proceedings*, 2022, pp. 1–8.
- [48] —, “SI-HDR-dataset for comparison of single-image high dynamic range reconstruction methods,” *University of Cambridge*, 2022.
- [49] X. Han, I. R. Khan, and S. Rahardja, “High Dynamic Range Image Tone Mapping: Literature review and performance benchmark,” *Digital Signal Processing*, p. 104015, 2023.
- [50] P.-H. Le, Q. Le, R. Nguyen, and B.-S. Hua, “Single-Image HDR Reconstruction by Multi-Exposure Generation,” in *Proceedings of the IEEE/CVF Winter Conference on Applications of Computer Vision*, 2023, pp. 4063–4072.
- [51] C. Bist, R. Cozot, G. Madec, and X. Ducloux, “Tone expansion using lighting style aesthetics,” *Computers & Graphics*, vol. 62, pp. 77–86, 2017.
- [52] Z. Khan, M. Khanna, and S. Raman, “FHDR: HDR Image Reconstruction from a Single LDR Image using Feedback Network,” in *2019 IEEE Global Conference on Signal and Information Processing (GlobalSIP)*. IEEE, 2019, pp. 1–5.
- [53] H. B. Barua, G. Krishnasamy, K. Wong, K. Stefanov, and A. Dhall, “ArtHDR-Net: Perceptually Realistic and Accurate HDR Content Creation,” in *2023 Asia Pacific Signal and Information Processing Association Annual Summit and Conference (APSIPA ASC)*. IEEE, 2023, pp. 806–812.
- [54] J. Li and P. Fang, “HDRNET: Single-Image-based HDR Reconstruction Using Channel Attention CNN,” in *Proceedings of the 2019 4th International Conference on Multimedia Systems and Signal Processing*, 2019, pp. 119–124.
- [55] M. S. Santos, T. I. Ren, and N. K. Kalantari, “Single Image HDR Reconstruction Using a CNN with Masked Features and Perceptual Loss,” *ACM Transactions on Graphics (TOG)*, vol. 39, no. 4, pp. 80–1, 2020.
- [56] G. Luzardo, J. Aelterman, H. Luong, S. Rousseaux, D. Ochoa, and W. Philips, “Fully-automatic inverse tone mapping algorithm based on dynamic mid-level tone mapping,” *APSIPA Transactions on Signal and Information Processing*, vol. 9, p. e7, 2020.
- [57] G. Cao, F. Zhou, K. Liu, A. Wang, and L. Fan, “A Decoupled Kernel Prediction Network Guided by Soft Mask for Single Image HDR Reconstruction,” *ACM Transactions on Multimedia Computing, Communications and Applications*, vol. 19, no. 2s, pp. 1–23, 2023.
- [58] B. Mildenhall, P. P. Srinivasan, M. Tancik, J. T. Barron, R. Ramamoorthi, and R. Ng, “NeRF: Representing Scenes as Neural Radiance Fields for View Synthesis,” *Communications of the ACM*, vol. 65, no. 1, pp. 99–106, 2021.
- [59] Y. Yang, J. Han, J. Liang, I. Sato, and B. Shi, “Learning Event Guided High Dynamic Range Video Reconstruction,” in *Proceedings of the IEEE/CVF Conference on Computer Vision and Pattern Recognition*, 2023, pp. 13 924–13 934.
- [60] B. Mildenhall, P. Hedman, R. Martin-Brualla, P. P. Srinivasan, and J. T. Barron, “NeRF in the Dark: High Dynamic Range View Synthesis from Noisy Raw Images,” in *Proceedings of the IEEE/CVF Conference on Computer Vision and Pattern Recognition*, 2022, pp. 16 190–16 199.
- [61] P. Raipurkar, R. Pal, and S. Raman, “HDR-cGAN: Single LDR to HDR Image Translation using Conditional GAN,” in *Proceedings of the Twelfth Indian Conference on Computer Vision, Graphics and Image Processing*, 2021, pp. 1–9.
- [62] S. Shin, K. Kong, and W.-J. Song, “CNN-based LDR-to-HDR conversion system,” in *2018 IEEE International Conference on Consumer Electronics (ICCE)*. IEEE, 2018, pp. 1–2.
- [63] A. S. Glassner, *An introduction to ray tracing*. Morgan Kaufmann, 1989.
- [64] T. Alotaibi, I. R. Khan, and F. Bourennani, “Quality Assessment of Tone-mapped Images Using Fundamental Color and Structural Features,” *IEEE Transactions on Multimedia*, 2023.
- [65] M. Narwaria, R. K. Mantiuk, M. P. Da Silva, and P. Le Callet, “HDR-VDP-2.2: A calibrated method for objective quality prediction of high dynamic range and standard images,” *Journal of Electronic Imaging*, vol. 24, no. 1, pp. 010 501–010 501, 2015.
- [66] B. Yan, B. Bare, and W. Tan, “Naturalness-aware deep no-reference image quality assessment,” *IEEE Transactions on Multimedia*, vol. 21, no. 10, pp. 2603–2615, 2019.
- [67] C. S. Ravuri, R. Sureddi, S. V. R. Dendi, S. Raman, and S. S. Channappaya, “Deep no-reference tone mapped image quality assessment,” in *2019 53rd Asilomar Conference on Signals, Systems, and Computers*. IEEE, 2019, pp. 1906–1910.
- [68] G. Kordopatis-Zilos, S. Papadopoulos, I. Patras, and I. Kompatsiaris, “ViSiL: Fine-grained Spatio-Temporal Video Similarity Learning,” in *Proceedings of the IEEE/CVF International Conference on Computer Vision*, 2019.
- [69] Y. Niu, J. Wu, W. Liu, W. Guo, and R. W. Lau, “HDR-GAN: HDR Image Reconstruction from Multi-Exposed LDR Images with Large Motions,” *IEEE Transactions on Image Processing*, vol. 30, pp. 3885–3896, 2021.
- [70] H. B. Barua, G. Krishnasamy, K. Wong, A. Dhall, and K. Stefanov, “HistoHDR-Net: Histogram Equalization for Single LDR to HDR Image Translation,” *arXiv preprint arXiv:2402.06692*, 2024.
- [71] HDRsoft, “Photomatix,” <https://www.hdrsoft.com/>, [Online; accessed 3-Nov-2023].
- [72] E. Reinhard, M. Stark, P. Shirley, and J. Ferwerda, “Photographic tone reproduction for digital images,” in *Seminal Graphics Papers: Pushing the Boundaries, Volume 2*, 2023, pp. 661–670.
- [73] R. Mantiuk, K. J. Kim, A. G. Rempel, and W. Heidrich, “HDR-VDP-2: A calibrated visual metric for visibility and quality predictions in all luminance conditions,” *ACM Transactions on graphics (TOG)*, vol. 30, no. 4, pp. 1–14, 2011.
- [74] Z. Wang and A. C. Bovik, “Mean squared error: Love it or leave it? A new look at Signal Fidelity Measures,” *IEEE signal processing magazine*, vol. 26, no. 1, pp. 98–117, 2009.
- [75] Z. Wang, A. C. Bovik, H. R. Sheikh, and E. P. Simoncelli, “Image Quality Assessment: From Error Visibility to Structural Similarity,” *IEEE transactions on image processing*, vol. 13, no. 4, pp. 600–612, 2004.
- [76] Z. Wang, L. Lu, and A. C. Bovik, “Video quality assessment based on structural distortion measurement,” *Signal processing: Image communication*, vol. 19, no. 2, pp. 121–132, 2004.
- [77] P. Gupta, P. Srivastava, S. Bhardwaj, and V. Bhateja, “A modified PSNR metric based on HVS for quality assessment of color images,” in *2011 International Conference on Communication and Industrial Application*. IEEE, 2011, pp. 1–4.
- [78] L. McInnes, J. Healy, and J. Melville, “Umap: Uniform manifold approximation and projection for dimension reduction,” *arXiv preprint arXiv:1802.03426*, 2018.
- [79] A. G. Howard, M. Zhu, B. Chen, D. Kalenichenko, W. Wang, T. Weyand, M. Andreetto, and H. Adam, “Mobilenets: Efficient convolutional neural networks for mobile vision applications,” *arXiv preprint arXiv:1704.04861*, 2017.
- [80] C. Szegedy, W. Liu, Y. Jia, P. Sermanet, S. Reed, D. Anguelov, D. Erhan, V. Vanhoucke, and A. Rabinovich, “Going deeper with convolutions,” in *Proceedings of the IEEE conference on computer vision and pattern recognition*, 2015, pp. 1–9.
- [81] K. Simonyan and A. Zisserman, “Very deep convolutional networks for large-scale image recognition,” *arXiv preprint arXiv:1409.1556*, 2014.
- [82] Y. Sun, W. Liu, Q. Bao, Y. Fu, T. Mei, and M. J. Black, “Putting People in their Place: Monocular Regression of 3D People in Depth,” in *Proceedings of the IEEE/CVF Conference on Computer Vision and Pattern Recognition*, 2022, pp. 13 243–13 252.
- [83] P. Patel, C.-H. P. Huang, J. Tesch, D. T. Hoffmann, S. Tripathi, and M. J. Black, “AGORA: Avatars in geography optimized for regression analysis,” in *Proceedings of the IEEE/CVF Conference on Computer Vision and Pattern Recognition*, 2021, pp. 13 468–13 478.
- [84] R. A. Güler, N. Neverova, and I. Kokkinos, “Densepose: Dense human pose estimation in the wild,” in *Proceedings of the IEEE conference on computer vision and pattern recognition*, 2018, pp. 7297–7306.
- [85] K. Lin, L. Wang, K. Luo, Y. Chen, Z. Liu, and M.-T. Sun, “Cross-domain complementary learning using pose for multi-person part segmentation,” *IEEE Transactions on Circuits and Systems for Video Technology*, vol. 31, no. 3, pp. 1066–1078, 2020.
- [86] M. Cordts, M. Omran, S. Ramos, T. Rehfeld, M. Enzweiler, R. Benenson, U. Franke, S. Roth, and B. Schiele, “The Cityscapes Dataset for Semantic Urban Scene Understanding,” in *Proceedings of the IEEE conference on computer vision and pattern recognition*, 2016, pp. 3213–3223.
- [87] A. Kirillov, E. Mintun, N. Ravi, H. Mao, C. Rolland, L. Gustafson, T. Xiao, S. Whitehead, A. C. Berg, W.-Y. Lo *et al.*, “Segment anything,” *arXiv preprint arXiv:2304.02643*, 2023.

GTA-HDR: A Large-Scale Synthetic Dataset for HDR Image Reconstruction

Supplementary Material

S1. INVERSE TONE MAPPING

Tone mapping [1]–[3] is the process of mapping the colors of HDR images capturing real-world scenes with a wide range of illumination levels to LDR images appropriate for standard displays with limited dynamic range. Inverse tone mapping [4] is the reverse process accomplished with either traditional (non-learning) methods or data-driven learning-based approaches. Fig. S1 illustrates an overview of the tone mapping pipeline and the process of inverse tone mapping using a data-driven learning-based model. Here, E is the sensor irradiance and Δt is the exposure time. The function $f_{crf}(E\Delta t)$ represents the tone mapping process, which outputs I_{LDR} images given I_{HDR} images captured by the camera sensor. The main goal of any HDR image reconstruction technique is to reverse the tone mapping process using another function $f_{crf}^{-1}(I_{LDR})/\Delta t$, which outputs reconstructed \hat{I}_{HDR} images given I_{LDR} images. The main challenge is that the steps in $f_{crf}(E\Delta t)$ are generally not reversible [5]. We can, however, approximate the reverse process with a data-driven learning-based model $f_{DL}(I_{LDR}, \Theta)$, which reconstructs \hat{I}_{HDR} images given I_{LDR} images, where Θ denotes the model parameters.

S2. HDR IMAGE RECONSTRUCTION

Fig. S2 illustrates examples of HDR images reconstructed by training ArtHDR-Net [6] with the GTA-HDR data in an end-to-end fashion. The histograms of the ground truth and the reconstructed images are also included. We can see that the histograms from the method trained with GTA-HDR data (*i.e.*, HDR_{Ours}) are more similar to the histograms of ground truth HDR images (*i.e.*, HDR_{GT}) than those from the method trained without GTA-HDR data (*i.e.*, HDR_{Base}). We also report the Kullback-Leibler (KL) divergence values for tone-mapped HDR_{GT} and tone-mapped HDR_{Base} and HDR_{Ours} using the RGB intensities. We see the average KL divergence of the RGB histogram intensity distributions are significantly lower for HDR_{Ours} compared to HDR_{Base} .

S3. SCENE DIVERSITY

Fig. S3 illustrates further qualitative results from the state-of-the-art method ArtHDR-Net [6] trained on GTA-HDR on extremely underexposed and overexposed images from a synthetic dataset. Similarly, Fig. S4 demonstrates the performance for arbitrary real images from the Internet. Both these cases show that GTA-HDR trained model is capable of recovering extremely over- and underexposed images with great fidelity. To further illustrate the contribution of the GTA-HDR dataset on in-the-wild HDR image reconstruction, in Fig. S5 we show

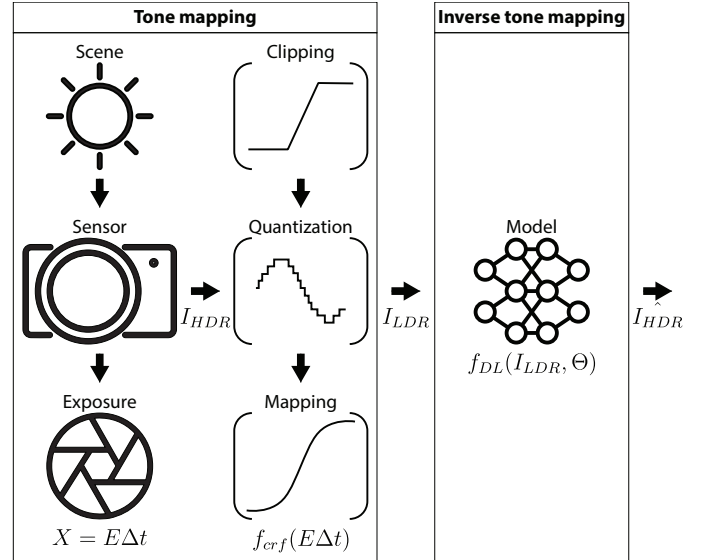


Fig. S1: **Tone mapping and inverse tone mapping processes.** The camera sensor function X is the product of the sensor irradiance E and exposure time Δt . The standard image formation pipeline (tone mapping) can be modeled with the function $f_{crf}(X)$, where $X = E\Delta t$. The goal of a data-driven inverse tone mapping model is to learn the function $f_{DL}(I_{LDR}, \Theta)$, where Θ are the model parameters, which correctly approximates the inverse of $f_{crf}(X)$.

the results on two images selected from HDR-Real [7] dataset having extreme lighting, color, and contrast variations. We also report the PSNR, SSIM, and HDR-VDP-2 scores.

S4. 3D HUMAN POSE AND SHAPE ESTIMATION

We used BEV [8] as a state-of-the-art pre-trained 3D human pose and shape estimator from images. We tested the BEV model on the reconstructed HDR images from several versions of the state-of-the-art method ArtHDR-Net [6]. Fig. S6 illustrates the contribution of GTA-HDR trained ArtHDR-Net using an end-to-end strategy for the task of 3D human pose and shape reconstruction. The figure demonstrates that the performance of the BEV 3D pose estimator is better in the case of an ArtHDR-Net reconstructed HDR image (capturing 4 people in the scene accurately) compared to the original LDR images (both under- and overexposed).

S5. HUMAN BODY PART SEGMENTATION

In this experiment, we used CDCL [9], a state-of-the-art body part segmentation model. Similar to the previous case,

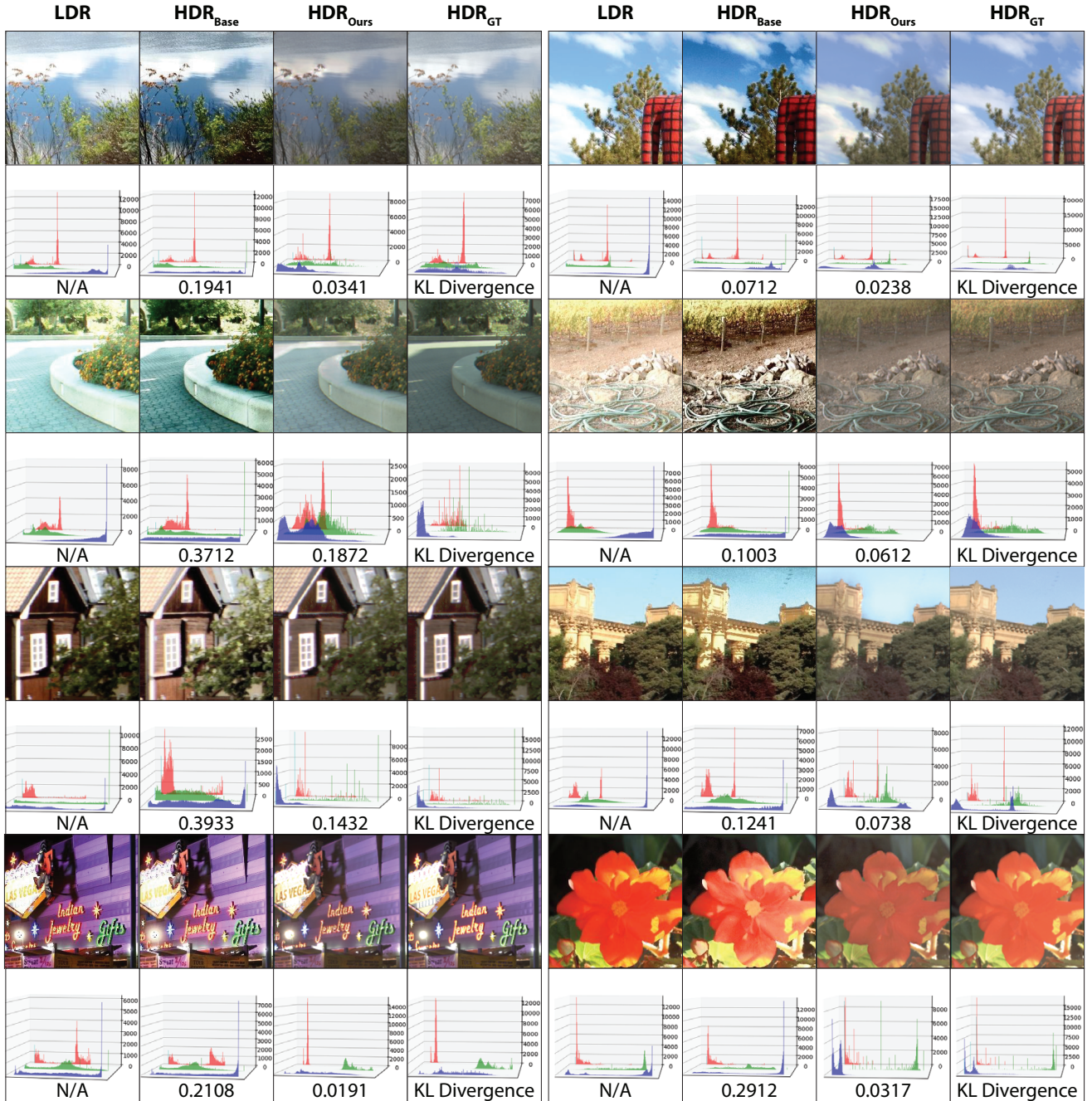


Fig. S2: HDR images reconstructed with and without GTA-HDR as part of the training dataset, along with the RGB histograms and KL-divergence values. *Base*: HDR images reconstructed with ArtHDR-Net [6] trained without GTA-HDR data; *Ours*: HDR images reconstructed with ArtHDR-Net trained with GTA-HDR data; *GT*: Ground truth.

we tested the model on reconstructed HDR images from several versions of ArtHDR-Net [6]. Fig. S7 illustrates the contribution of the GTA-HDR dataset to this task. The human body part segmentation results are more accurate with the reconstructed HDR images than the over- or underexposed LDR images. For the overexposed LDR images, one person is completely missed in the second image. For the underexposed LDR images, the output is noisy and erroneous. Finally, the processed HDRs using ArtHDR-Net [6] trained with the GTA-HDR dataset deliver the most accurate segments.

S6. SEMANTIC SEGMENTATION

Finally, we report an experiment on another vision task, *i.e.*, holistic semantic segmentation of scenes, which is an important task in robotics and human-robot interaction. We consider a recent state-of-the-art method called SAM [10] as a pre-trained holistic scene segmentation model. Fig. S8 illustrates the impact of the GTA-HDR trained model ArtHDR-Net [6]. The objects/buildings in the background are not segmented well in the overexposed LDR images. Similarly, in the underexposed LDR images, even the near objects

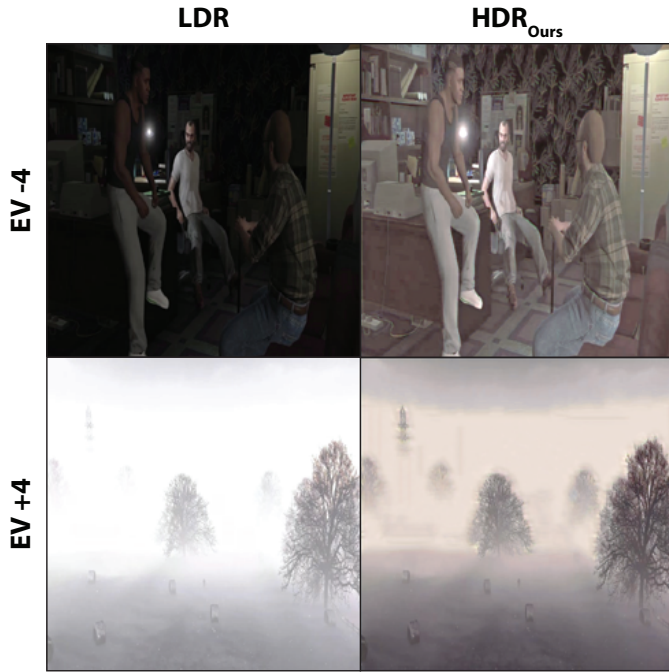


Fig. S3: **Performance of ArtHDR-Net [6].** The state-of-the-art method was trained with the GTA-HDR dataset and used for HDR image reconstruction from highly overexposed and underexposed synthetic LDR images. *EV*: Exposure value; *Ours*: HDR images reconstructed with ArtHDR-Net trained with GTA-HDR data.

are sometimes segmented erroneously. However, in the HDR images, these issues have been mitigated to a great extent.

REFERENCES

- [1] X. Han, I. R. Khan, and S. Rahardja, “High Dynamic Range Image Tone Mapping: Literature review and performance benchmark,” *Digital Signal Processing*, p. 104015, 2023.
- [2] A. Rana, G. Valenzise, and F. Dufaux, “Learning-based tone mapping operator for efficient image matching,” *IEEE Transactions on Multimedia*, vol. 21, no. 1, pp. 256–268, 2018.
- [3] A. Ak, A. Goswami, W. Hauser, P. Le Callet, and F. Dufaux, “RV-TMO: Large-Scale Dataset for Subjective Quality Assessment of Tone Mapped Images,” *IEEE Transactions on Multimedia*, 2022.
- [4] L. Wang and K.-J. Yoon, “Deep Learning for HDR Imaging: State-of-the-Art and Future Trends,” *IEEE transactions on pattern analysis and machine intelligence*, vol. 44, no. 12, pp. 8874–8895, 2021.
- [5] P.-H. Le, Q. Le, R. Nguyen, and B.-S. Hua, “Single-Image HDR Reconstruction by Multi-Exposure Generation,” in *Proceedings of the IEEE/CVF Winter Conference on Applications of Computer Vision*, 2023, pp. 4063–4072.
- [6] H. B. Barua, G. Krishnasamy, K. Wong, K. Stefanov, and A. Dhall, “ArtHDR-Net: Perceptually Realistic and Accurate HDR Content Creation,” in *2023 Asia Pacific Signal and Information Processing Association Annual Summit and Conference (APSIPA ASC)*. IEEE, 2023, pp. 806–812.
- [7] Y.-L. Liu, W.-S. Lai, Y.-S. Chen, Y.-L. Kao, M.-H. Yang, Y.-Y. Chuang, and J.-B. Huang, “Single-Image HDR Reconstruction by Learning to Reverse the Camera Pipeline,” in *Proceedings of the IEEE/CVF Conference on Computer Vision and Pattern Recognition*, 2020, pp. 1651–1660.
- [8] Y. Sun, W. Liu, Q. Bao, Y. Fu, T. Mei, and M. J. Black, “Putting People in their Place: Monocular Regression of 3D People in Depth,” in *Proceedings of the IEEE/CVF Conference on Computer Vision and Pattern Recognition*, 2022, pp. 13 243–13 252.
- [9] K. Lin, L. Wang, K. Luo, Y. Chen, Z. Liu, and M.-T. Sun, “Cross-domain complementary learning using pose for multi-person part segmentation,”

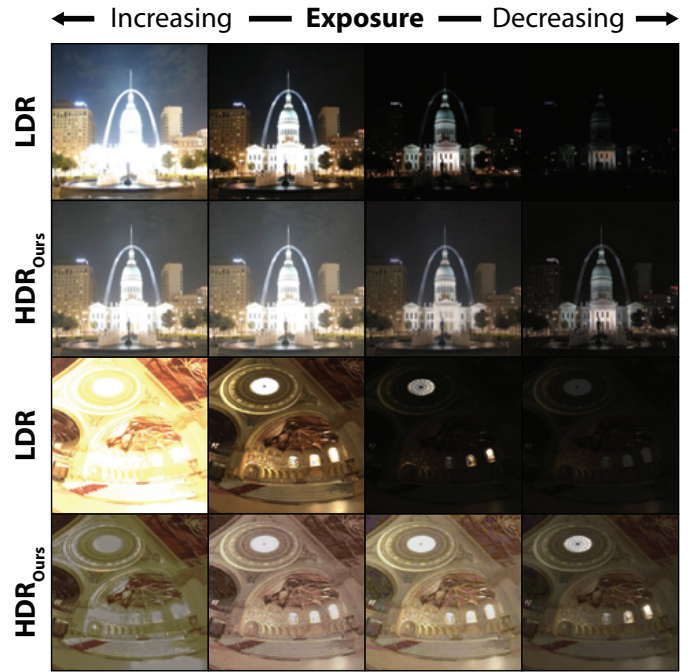


Fig. S4: **Performance of ArtHDR-Net [6].** The state-of-the-art method was trained with the GTA-HDR dataset and used for HDR image reconstruction from highly overexposed and underexposed real LDR images from the Internet. *Ours*: HDR images reconstructed with ArtHDR-Net trained with GTA-HDR data.

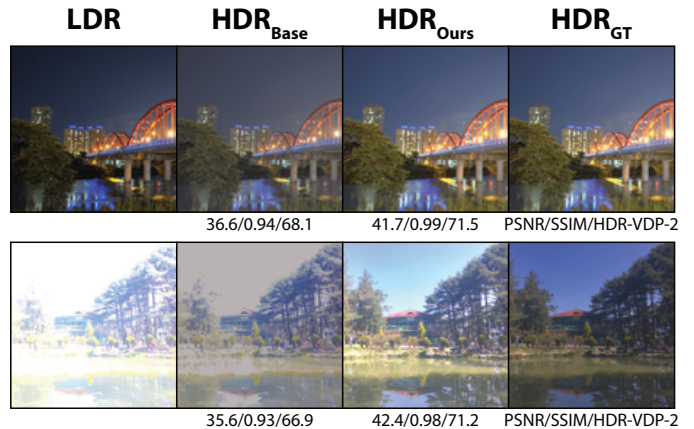


Fig. S5: **Performance of ArtHDR-Net [6].** We show the results on two extreme real in-the-wild images selected from HDR-Real [7] dataset. These images have extreme lighting conditions, color variations, and contrast levels. *Base*: HDR images reconstructed with ArtHDR-Net trained without GTA-HDR data; *Ours*: HDR images reconstructed with ArtHDR-Net trained with GTA-HDR data; *GT*: Ground truth.

IEEE Transactions on Circuits and Systems for Video Technology, vol. 31, no. 3, pp. 1066–1078, 2020.

- [10] A. Kirillov, E. Mintun, N. Ravi, H. Mao, C. Rolland, L. Gustafson, T. Xiao, S. Whitehead, A. C. Berg, W.-Y. Lo *et al.*, “Segment anything,” *arXiv preprint arXiv:2304.02643*, 2023.

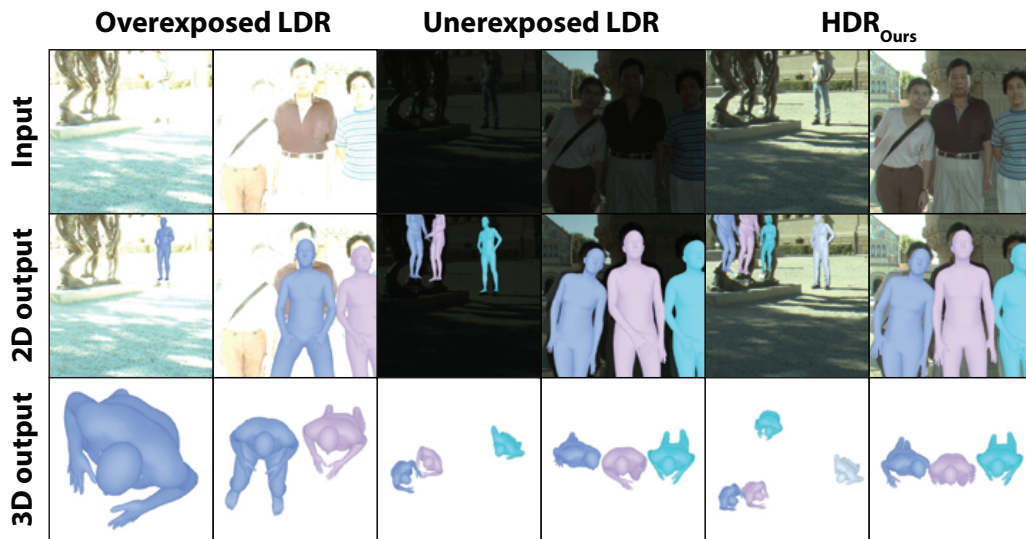


Fig. S6: **Impact of the GTA-HDR dataset on the performance of the state-of-the-art 3D human pose and shape estimation.** We used ArtHDR-Net [6] trained with the GTA-HDR dataset for HDR image reconstruction from under- and overexposed LDR images. The resulting HDR images were used by BEV [8] for 3D human pose and shape estimation. *Ours*: HDR images reconstructed with ArtHDR-Net trained with GTA-HDR data.



Fig. S7: **Impact of the GTA-HDR dataset on the performance of the state-of-the-art in 2D human body part segmentation.** We used ArtHDR-Net [6] trained with the GTA-HDR dataset for HDR image reconstruction from under- and overexposed LDR images. The resulting HDR image was used by CDCL [9] for 2D human body part segmentation. *Ours*: HDR images reconstructed with ArtHDR-Net trained with GTA-HDR data.

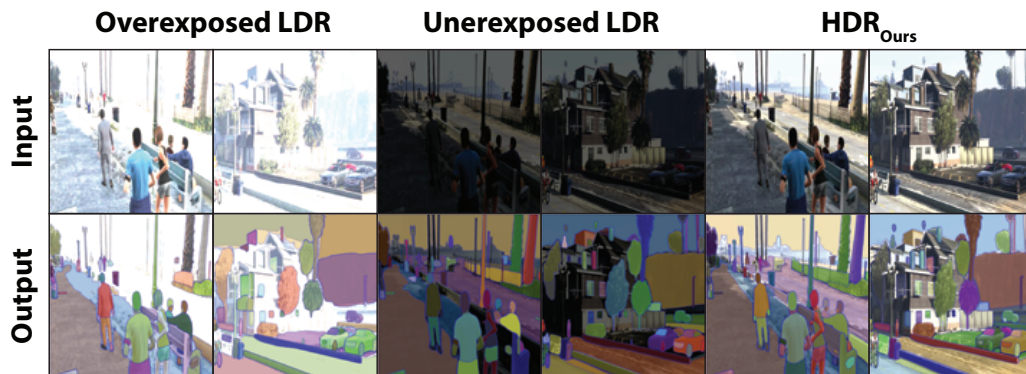


Fig. S8: **Impact of the GTA-HDR dataset on the performance of the state-of-the-art in semantic segmentation.** We used ArtHDR-Net [6] trained with the GTA-HDR dataset for HDR image reconstruction from under- and overexposed LDR images. The resulting HDR image was used by SAM [10] for semantic segmentation. *Ours*: HDR images reconstructed with ArtHDR-Net trained with GTA-HDR data